Spring net community production and its coupling with the CO_2 dynamics in the surface water of the northern Gulf of Mexico

Zong-Pei Jiang[1,2], Wei-Jun Cai[2*], John Lehrter[3], Baoshan Chen[2], Zhangxian Ouyang[2], Chenfeng Le[1], Brian J. Roberts[4], Najid Hussain[2], Michael K. Scaboo[2], Junxiao Zhang[5], Yuanyuan Xu[2]

[1]Ocean College, Zhejiang University, Zhoushan, Zhejiang, China
[2]School of Marine Science and Policy, University of Delaware, Newark, Delaware, USA
[3]University of South Alabama, Alabama, USA
[4]Louisiana Universities Marine Consortium, Louisiana, USA
[5]South China Sea Marine Survey and Technology Center, State Oceanic Administration, Guangzhou, Guangdong, China

Correspondence to: Wei-Jun Cai (wcai@udel.edu)

Abstract. Net community production (NCP) in the surface water of the northern Gulf of Mexico (nGOM) and its coupling with the CO_2 system were examined during the productive spring season. NCP was estimated using multiple approaches: 1) underway O_2 and Ar ratio, 2) oxygen changes during light/dark bottle oxygen incubations, and 3) non-conservative changes in dissolved inorganic carbon or nutrients. These methods all showed high spatial variability of NCP and displayed similar patterns along the river-ocean mixing gradient showing high production rates in plume regions. NCP_{O2Ar} estimated from high-resolution O_2 and Ar underway measurement indicated heterotrophic conditions at the high-nutrient and high-turbidity Mississippi river end (-51.3 ± 11.9 mmol C m^{-2} d^{-1} when salinity < 2) resulting from the influence of terrestrial carbon input and light limitation on photosynthesis. High NCP_{O2Ar} rates (105.0 ± 59.2 mmol C m^{-2} d^{-1}, up to 235.4 mmol C m^{-2} d^{-1}) were observed in the Mississippi and Atchafalaya plumes at intermediate salinities between 15 and 30 where light and nutrient were both favorable for phytoplankton production. NCP_{O2Ar} rates observed in the high-salinity, oligotrophic offshore waters (salinity > 35.5) were close to zero due to nutrient limitation. Air-sea CO_2 fluxes generally showed corresponding changes from being a strong CO_2 source in the river channel (55.5 ± 7.6 mmol C m^{-2} d^{-1}), to a CO_2 sink in the plume (-13.4 ± 5.5 mmol C m^{-2} d^{-1}), and to be nearly in equilibrium with the atmosphere in offshore waters. Overall, the surface water of the nGOM was net autotrophic during spring 2017 with an area-weighted mean NCP_{O2Ar} of 21.2 mmol C m^{-2} d^{-1} and was a CO_2 sink of -6.7 mmol C m^{-2} d^{-1}. A temporal mismatch between *in situ* biological production and gas exchange of O_2 and CO_2 was shown through a box model to result in decoupling between NCP_{O2Ar} and CO_2 flux (e.g., autotropic water as a CO_2 source outside the Mississippi River mouth and heterotopic water as a CO_2 sink in the Atchafalaya coastal water). This decoupling was a result of *in situ* biological production superimposed on the lingering background pCO_2 from the source water because of the slow air-sea CO_2 exchange rate and the buffering effect of the carbonate system.

1

1 Introduction

The continental shelf is among the most biologically active areas of the biosphere and plays a significant role in global biogeochemical cycles (Chen and Borges, 2009; Chen and Swaney, 2012; Gattuso et al., 1998; Muller-Karger et al., 2005). Despite its moderate surface area (~7 %), the continental shelf accounts for 14-30 % of net ecosystem production (Gattuso et

5   al., 1998), 80 % of organic matter burial (Gattuso et al., 1998), and 15-21 % of the CO_2 uptake of the global ocean (Cai, 2011; Cai et al., 2006; Chen and Borges, 2009; Laruelle et al., 2010). Moreover, anthropogenic impacts have substantially changed the nutrient and carbon loads delivered to the coastal oceans (Bauer et al., 2013; Regnier et al., 2013; Yang et al., 2018), which have in turn resulted in a series of environmental problems (e.g., coastal eutrophication, hypoxia, and acidification) in some coastal regions (Cai et al., 2011; Diaz and Rosenberg, 2008; Rabalais et al., 2014; Wallace et al.,

10   2014). Understanding and quantifying how these impacts affect the metabolic balance and CO_2 fluxes of coastal systems is of critical interest to scientists and policy-makers. However, the substantial heterogeneity resulting from physical and biogeochemical interactions makes assessing metabolic state and carbon flux a challenging task in dynamic coastal environments.

Net community production (NCP) is defined as the difference between gross primary production and community respiration

15   and indicates whether the ecosystem is a net source or sink of organic matter (Eppley and Peterson, 1979; Sarmiento and Gruber, 2006). NCP in the mixed layer plays an important role in regulating the surface CO_2 and O_2 dynamics. It also represents the amount of organic carbon available for export to the subsurface, which is closely related to bottom-water biogeochemical processes, e.g., the development and maintenance of hypoxia.

The northern Gulf of Mexico (nGOM) is a river-dominated continental shelf (Mckee et al., 2004) with NCP and CO_2

20   dynamics significantly affected by the terrestrial inputs of carbon and nutrients from the Mississippi-Atchafalaya River system (Lohrenz et al., 2014). CO_2 variability in the nGOM was extensively investigated by high-resolution underway measurement of the partial pressure of CO_2 (pCO_2) (Huang et al., 2015). High terrestrial inorganic and organic carbon loading results in CO_2 oversaturation and net CO_2 efflux to the atmosphere in the river channel and estuary of the Mississippi River (Cai, 2003; Guo et al., 2012; Huang et al., 2015; Lohrenz et al., 2010). On the continental shelf, reduced pCO_2

25   observed in the Mississippi plume (sink for atmospheric CO_2) was attributed to strong primary production supported by the

excessive riverine nutrient loads (Guo et al., 2012; Huang et al., 2015; Lohrenz et al., 1990; 1999; 2014). Enhanced surface production and subsequent subsurface respiration of the sinking organic matter has led to recurring bottom-water hypoxia covering large portions of the Louisiana-Texas shelf in summer when stratification limits O_2 replenishment (Bianchi et al., 2010; Obenour et al., 2013; Rabalais et al., 2002). Springtime riverine nutrient flux and subsequent biological production in

5   surface water play a critical role in determining the size of the summertime bottom-water hypoxia area in the nGOM (Justić et al., 1993; Turner et al., 2012). Rapid subsurface respiration also leads to a significant decrease in pH and a weakening of acid-base buffer capacity, which further results in enhancing the coastal ocean acidification problem (Cai et al., 2011). Previous NCP studies in the nGOM have been mainly based on dissolved oxygen changes during light/dark bottle oxygen incubations and non-conservative removal of dissolved inorganic carbon or nutrients (Cai, 2003; Huang et al., 2012; Guo et

10 al., 2012; Murrell et al., 2009; 2013). However, the detailed relationship between NCP and CO_2 dynamics remains unclear because of the low spatial resolution of the conventional NCP measurements based on discrete samples. In this study, we present the first attempt to obtain high-resolution NCP_{O2Ar} estimates from continuous underway measurement of oxygen to argon ratio (O_2/Ar) in the nGOM in spring. The NCP_{O2Ar} result was compared to those derived from traditional approaches to evaluate the consistency of NCP estimates from various methods. Meanwhile, these NCP methods are associated with different

15 temporal and spatial scales and are differently affected by biological and physical processes. By comparing NCP estimates from multiple methods we can get a more robust understanding of the overall metabolism of the system. The simultaneous underway determination of NCP_{O2Ar} and pCO_2, together with measurements of dissolved oxygen (DO), dissolved inorganic carbon (DIC), total alkalinity (TA), nutrients, and other environmental parameters, allow us to better constrain the variability and controls on the metabolic balance and CO_2 flux in the nGOM. We also use a box model to investigate the relationship

20 between NCP and air-sea fluxes of O_2 and CO_2.

2 Methods

2.1 Sample collection and measurements

The cruise was conducted onboard *RV Pelican* during 6-16 April 2017. The study region covered the northern Gulf of Mexico including the Mississippi and Atchafalaya estuaries and the adjacent Louisiana continental shelf where summer hypoxia

repeatedly occurs (Fig. 1). Vertical water column profiles of temperature, salinity, DO, chlorophyll fluorescence (Chl-a), and photosynthetically active radiation (PAR) were measured by a Sea-Bird CTD system (SBE 911plus) at 83 sampling stations (Fig. 1). Discrete water samples for DIC, TA, DO, and nutrients ($n = 382$) were collected from 3-12 depths depending on the bottom depth and vertical profiles of temperature, salinity and DO. River water samples of the Mississippi (89.98° W, 29.85°

5 N) and Atchafalaya (91.21° W, 29.70° N, Fig. 1) were taken on 5 April, one day prior to the cruise, to identify the DIC and TA concentrations of the river end-members. Samples for DIC and TA were collected in 250 mL borosilicate glass bottles and preserved with 50 μl of saturated $HgCl_2$ solution (Dickson et al., 2007). DIC was measured by non-dispersive infrared measurement on the CO_2 stripped from the acidified sample (AS-C3, Apollo SciTech). TA titrations were conducted with a ROSS[TM] combination electrode 8102 (Thermo Fisher Scientific) on a semi-automated titrator (AS-ALK2, Apollo SciTech).

10 The precision of DIC and TA measurements were both 2 μmol kg^{-1}. DIC and TA measurements were calibrated, both with accuracy better than 0.1 %, with certified reference materials provided by A. G. Dickson, Scripps Institution of Oceanography. DO in discrete samples was measured by a Shimadzu UV-1700 at 25 °C using the spectrophotometric method following Pai et al. (1993) with an accuracy of 0.2 %. For nutrient analysis, water from each Niskin bottle was immediately filtered through 0.22 μm, sterile, polyethersulfone syringe filters and stored frozen for subsequent nutrient characterization. Samples were

15 analyzed in duplicate for dissolved NO_x ($NO_3^- + NO_2^-$) by Cu-Cd reduction followed by azo dye colorimetry using a Lachat Instruments QuikChem® FIA+ 8000 Series Automated Ion Analyzer at the Louisiana Universities Marine Consortium as described previously (Roberts and Doty, 2015). Standard curves were prepared using standard NO_3-N and NO_2-N stock solutions (Hach, Loveland CO) and yielded r^2 values of ≥ 0.999.

2.2 Underway measurements

20 The underway system was fed by the ship's seawater supply from an inlet located at an approximate depth of 2.5 m. The flow-through system and the Multiple Instrument Data Acquisition System (MIDAS) provided measurements on sea surface temperature, conductivity (Sea-Bird SBE 21 Thermosalinograph), Chl-a (Turner Model 10 Series Fluorometers), and light transmittance (WETLabs 25-cm path length transmissometer). MIDAS also integrated data from the ship's meteorological suite: wind, barometric pressure, temperature, and relative humidity (R.M. Young) and PAR (LI-COR LI-190SZ).

Underway seawater pCO_2 was measured with a precision of 0.1 µatm by an automated flow-through pCO_2 measuring system (AS-P2, Apollo SciTech) with a shower head equilibrator and a non-dispersive infrared gas detector (LI-7000, LI-COR) (Huang et al., 2015). The pCO_2 measurement was calibrated twice daily against 3 certified gas standards (150.62, 404.72, and 992.54 ppm) and the accuracy was better than ±2 µatm. The underway pCO_2 system alternated measurements on a

5   stream of seawater split from the same inlet for the MIDAS and a stream of outside air from the bow of the vessel away from chimney contamination. The atmospheric pCO_2 was measured every 3 hours automatically. The underway DO was measured by an Aanderaa 4835 optode which was calibrated against discrete surface water values by spectrophotometric measurements.

Underway high-resolution measurements of O_2/Ar were made by equilibrator inlet mass spectrometry as described by Cassar

10   et al. (2009). Briefly, a fraction of underway seawater (the same supplied to the pCO_2 measuring system) was pumped through a gas-permeable membrane contactor cartridge at a flow rate of 100 mL min^{-1}. The cartridge was connected to a quadrupole mass spectrometer (Pfeiffer Prisma) through a fused-silica capillary which continuously sampled headspace gases for O_2/Ar measurement. As atmospheric O_2/Ar is essentially constant relative to that in the surface water, calibrations of the O_2/Ar ion current ratio were conducted by sampling the ambient air every 3 hours through a second capillary (Cassar

15   et al., 2009). The instrument precision estimated from the repeated measurements of atmospheric O_2/Ar was 0.3 %.

2.3 Calculations

The mixed layer depth (MLD) was defined as the depth at which the density changed by 0.03 kg m^{-3} relative to the surface value and was calculated according to the density profiles at sampling stations. Air-sea CO_2 flux (F_{CO2}) was calculated as:

$$F_{CO2} = k_{CO2} \ K_0 \ \Delta pCO_{2(sea\text{-}air)} = k_{CO2} \ K_0 \left(pCO_{2meas} - pCO_{2air} \right) \quad (1)$$

20   where k_{CO2} is the gas transfer velocity of CO_2 calculated using the daily mean wind speed from the three-dimensional Coupled Ocean/Atmosphere Mesoscale Prediction System (COAMPS) (Hodur, 1997) and the coefficients of Sweeney et al. (2007). The COAMPS daily wind speed agreed well (mean difference = 0.4 m s^{-1}, figure not shown) with buoy measurements in our study region (s42047, s8768094, FRWL1, MRSL1, LOPL1, GISL1, PSTL1, and PILL1, data from the National Data Buoy Center, http://www.ndbc.noaa.gov/maps/WestGulf.shtml). K_0 is the CO_2 solubility coefficient calculated

from the measured sea surface temperature and salinity (Weiss, 1974). $\Delta pCO_{2(sea-air)}$ is the difference between the measured pCO_2 in the surface water (pCO_{2meas}) and in the atmosphere (pCO_{2air}). pCO_{2air} variability was negligible (405 ± 4 µatm) compared to the large variations in pCO_{2meas} (110-1800 µatm), so pCO_{2air} was set at the cruise average value of 405 µatm for all flux calculations. Negative F_{CO2} values correspond to net CO_2 uptake by the ocean (ocean as a CO_2 sink for the

5   atmosphere). Air-sea O_2 flux (F_{O2}) was calculated as:

$$F_{O2} = k_{O2}\ \Delta O_{2(sea-air)} = k_{O2}\left([O_2]_{meas} - [O_2]_{sat}\right) \quad (2)$$

where k_{O2} is the gas exchange velocity of O_2 which was calculated in a similar way with that of k_{CO2}, $\Delta O_{2(sea-air)}$ is the difference between the seawater DO concentration from the calibrated underway optode measurement ($[O_2]_{meas}$) and the saturated DO concentration ($[O_2]_{sat}$) calculated from the measured sea surface temperature and salinity (Garcia and Gordon,

10   1992). The oxygen saturation percentage (DO%) is calculated as DO% = $[O_2]_{meas}/[O_2]_{sat}$.

2.4 NCP estimates

In this study, NCP rates were estimated by three different approaches: underway O_2/Ar measurements (NCP_{O2Ar}), light/dark bottle dissolved oxygen (DO) incubations ($NCP_{DO\text{-}incub}$), and non-conservative changes in DIC ($NCP_{\Delta DIC}$) or NO_x ($NCP_{\Delta NOx}$).

NCP from the O_2/Ar method: DO concentration in the surface water is affected by physical (e.g., changes in temperature,

15   salinity, atmospheric pressure, and bubble dissolution and injection) and biological processes (e.g., photosynthesis and respiration). Ar and O_2 have similar responses to physical processes as they have similar solubility and temperature dependency (Garcia and Gordon, 1992; Hamme and Emerson, 2004). However, Ar is biologically inert and can therefore be used to infer abiotic influences on oxygen. Contemporaneous measurements of O_2 and Ar thus allow the biologically induced O_2 changes to be isolated (Craig and Hayward, 1987). By measuring the biologically mediated oxygen supersaturation $\Delta(O_2/Ar)$ (Cassar

20   et al., 2011; Craig and Hayward, 1987; Jonsson et al., 2013; Kaiser et al., 2005):

$$\Delta(O_2/Ar) = \frac{[O_2]/[Ar]}{[O_2]_{sat}/[Ar]_{sat}} - 1 \quad (3)$$

the surface NCP can be approximated by the net air-sea biological oxygen flux (bioflux, mmol O_2 m^{-2} d^{-1}) under a physically isolated mixed layer assumption (Jonsson et al. 2013):

6

$$NCP_{O2Ar} = bioflux = k_{O2}[O_2]_{sat}\Delta(O_2/Ar) \quad (4)$$

The modeling study by Teeter et al. (2018) suggested that the bioflux accurately represents the exponentially weighted NCP over the past several residence times of O_2. The residence times of O_2 (MLD/gas transfer velocity of O_2, ~2.3 days during our cruise) refers to the length of time required to exchange O_2 between the mixed layer and the atmosphere (Kaiser et al., 2005; Teeter et al., 2018). To account for the wind speed history prior to the arrival of the ship at each station, the weighting technique of Reuer et al. (2007) modified by Teeter et al. (2018) was applied to calculate the gas exchange velocity of O_2 in this study.

NCP from the DO incubation: NCP was estimated by the light/dark bottle incubation method at 43 CTD stations (Fig. 1). Surface water samples (~1.5 m) were collected from Niskin bottles into triplicate clear and black 300-ml Wheaton BOD bottles. The initial oxygen saturation percentage and temperature in each bottle was measured by inserting a luminescent/optical dissolved oxygen probe (Hach LDO101, Hach Hq40d meter) into the bottle. Care was taken to avoid introducing air bubbles during this step. After recording the initial oxygen saturation percentage value, the probe was removed and the small volume displaced by the probe (~3 ml) was replaced with filtered seawater from an offshore, low nutrient site. The addition of DO to the bottle from the replacement water was considered small, on the order of the method detection limit of approximately 2 mmol m^{-3} d^{-1} (Murrell et al. 2009; 2013). Clear and dark bottles were placed into a deck incubator screened at 50 % of ambient sunlight for 24 hours. The deck incubator was plumbed with flowing seawater from the MIDAS in order to maintain surface water temperatures. After 24 hours, the oxygen saturation percentage and temperature were measured again with the oxygen probe. DO concentrations obtained from the LDO probe were verified by a comparison with DO concentrations measured by the spectrophotometric method of Pai et al. (1993) in a subset of samples ($n = 14$). The mean difference between the two methods of ±5 % was consistent with previous comparisons of probe measured versus Winkler measured DO based on several hundred comparisons (Murrell et al. 2013).

The respiration rate was calculated from the DO changes in the dark bottles (R_{dark}, mmol O_2 m^{-3} d^{-1}). The respiration rate was assumed to be uniform in the mixed layer, thus, the integrated respiration over the MLD ($Resp_{Int}$, mmol O_2 m^{-2} d^{-1}) was calculated as $Resp_{Int} = R_{dark}$*MLD. The gross primary production (GPP) varied with depth due to the reduction in light availability with increasing depth. The mean percentage of PAR (%PAR) in the water column in relation to surface PAR (E_0) was calculated at each station as:

$$\%PAR = \frac{E_0}{K_d MLD}(1 - e^{(-K_d MLD)}) \quad (5)$$

where E_0 is 100 %, light attenuation (K_d, m^{-1}) is the rate of exponential decline in PAR as a function of depth as measured by the CTD. In our study, we assumed that GPP was linearly dependent on light up to a maximum GPP$_{max}$ occurred when %PAR = 50 %. This assumption is based on previous measurements from this shelf that indicate photosynthesis begins to saturate at

5 light level of ~200 µmol quanta m^{-2} s^{-1} (Lohrenz et al., 1994), which is roughly 50 % of light in the surface mixed layer (Lohrenz et al., 1999). GPP$_{max}$ was thus estimated as GPP$_{max}$ = R$_{light}$ - R$_{dark}$, where R$_{light}$ is the DO change rate in the light bottles. To calculate the integrated GPP in the mixed layer (GPP$_{Int}$, mmol O$_2$ m^{-2} d^{-1}), the GPP was scaled by the light environment in the MLD:

if %PAR $\geq$ 50 %, GPP$_{Int}$ = GPP*MLD   (6)

10 if %PAR < 50 %, GPP$_{Int}$ = 2*%PAR*GPP*MLD   (7)

The coefficient 2 in Eq. 7 was used so that the product of 2*%PAR would scale from 0 to 1, i.e., GPP approaches GPP$_{max}$ at %PAR = 50 %. Finally, the NCP integrated over the MLD (NCP$_{DO-incub}$, mmol O$_2$ m^{-2} d^{-1}) was estimated as:

NCP$_{DO-incub}$ = (GPP$_{Int}$ - Resp$_{Int}$)   (8)

The mean standard error of NCP$_{DO-incub}$ estimates from triplicate bottle incubations across all sites were approximately 16 %

15 of the mean rates.

NCP from the non-conservative changes in DIC or nutrients: NCP can also be estimated from the biologically induced deviations of DIC or nutrients from conservative mixing. We applied a three end-member mixing model (Huang et al., 2012) to distinguish the contribution from conservative mixing (X_{mix}) and the biologically induced change (ΔX_{biol}). The X_{mix} was calculated from the fractions of Gulf of Mexico surface seawater (f_{sw}), Mississippi River water (f_{MR}), and Atchafalaya River

20 water (f_{AR}) together with the corresponding end-member concentrations shown in Table 1:

$1 = f_{sw} + f_{MR} + f_{AR}$ (9)

$X_{mix} = X_{sw}*f_{sw} + X_{MR}*f_{MR} + X_{AR}*f_{AR}$ (10)

We used salinity and potential alkalinity (PTA = TA + NO$_x$) (Brewer and Goldman, 1976) as the two conservative tracers to constrain f_{sw}, f_{MR}, and f_{AR} using a non-negative least square method (Lawson and Hanson, 1974). The concentrations of DIC$_{mix}$

and NO_{xmix} from conservative mixing can then be calculated from Eq. 10, and the biologically induced changes in DIC (ΔDIC_{NCP}) and NO_x (ΔNO_{xNCP}) were estimated as:

$$\Delta DIC_{NCP} = DIC_{meas} - DIC_{mix} - \Delta DIC_{gas} \quad (11)$$

$$\Delta NO_{xNCP} = NO_{xmeas} - NO_{xmix} \quad (12)$$

5   where DIC_{meas} and NO_{xmeas} are the observed concentrations of DIC and NO_x, and ΔDIC_{gas} is the DIC changes induced by air-sea CO_2 exchange. Note that ΔDIC_{NCP} (mmol C m^{-3}) and ΔNO_{xNCP} (mmol N m^{-3}) represent the cumulative NCP-induced changes in the concentrations of DIC and NO_x since the mixing of river water with oceanic water. In order to calculate the NCP rates derived from DIC ($NCP_{\Delta DIC}$, mmol C m^{-2} d^{-1}) or NO_x ($NCP_{\Delta NOx}$, mmol N m^{-2} d^{-1}), the MLD and plume residence time (τ) need to be considered (Cai, 2003):

10    $$NCP_{\Delta DIC} = \Delta DIC_{NCP}*MLD/\tau \quad (13)$$

$$NCP_{\Delta NOx} = \Delta NO_{xNCP}*MLD/\tau \quad (14)$$

To facilitate comparison with previous studies (Guo et al., 2012, Huang et al., 2012, Cai, 2003), τ values for the Mississippi plume were taken from Green et al. (2006) as 1, 1.5, and 6 days for salinity range of 0-18, 18-27, and 27-34.5 respectively. In our study, we only calculated $NCP_{\Delta DIC}$ and $NCP_{\Delta NOx}$ for stations in the Mississippi plume because τ for the Atchafalaya plume

15   is not available.

NCP unit conversion: To facilitate the comparison of NCP estimates from the different approaches, NCP rates were converted to the same carbon units (mmol C m^{-2} d^{-1}) using the Redfield ratio of $C:N:O_2 = 106:16:138$. The photosynthetic molar ratio of $C:O_2$ for new and recycled production may vary between 1.1 (NH_4^+ as nitrogen source) and 1.4 (NO_3^- as nitrogen source) (Laws, 1991). In our study region, the riverine input of NO_3^- was the main nitrogen source for biological uptake (Table 1) and

20   we considered the average Redfield ratio of $C:O_2 = 106:138$ to be appropriate. Although biological C:N uptake may differ from the Redfield stoichiometry (Geider and La Roche, 2002; Sambrotto et al., 1993), the applicability of the Redfield C:N ratio has been previously demonstrated in our study region (Huang et al., 2012; Xue et al., 2015) and confirmed in this study.

2.5 Box model for NCP and gas exchange

A simple box model was used to examine the relationship between NCP and air-sea fluxes of O_2 and CO_2. The environmental settings of the box model were taken from the averaged condition during our study period: temperature = 22 °C, salinity = 35, TA = 2400 µmol L^{-1}, pCO_{2air} = 405 µatm, MLD = 6 m, and wind speed = 6 m s^{-1}. The initial state of the seawater was set to be in equilibrium with the atmosphere, and the concentrations of DO and pCO_2 in the seawater were modulated by time-dependent NCP functions and air-sea gas exchange at hourly time steps. At each time step, the relative changes in concentrations of DIC, TA, and DO resulting from NCP were assumed to follow the ratio of 106:17:138 (Zeebe and Wolf-Gladrow, 2001). The pCO_2 was calculated from DIC and TA using the CO2SYS program (Pierrot and Wallace, 2006). The air-sea flux of O_2 and CO_2 were calculated following Eq. 1 and Eq. 2.

3 Results

3.1 General hydrological and biogeochemical characteristics

The Mississippi and Atchafalaya Rivers typically experience peak discharge and NO_x loading in spring (Fig. S1). These peaks in spring 2017 occurred later than the average condition during 1997-2017 and the monthly mean values of discharge and NO_x loading in April 2017 were slightly lower than the long-term mean values (Fig. S1). Surface water parameters (temperature, salinity, light transmittance, Chl-a, DO%, pCO_2, and $\Delta O_2/Ar$) showed high spatial variability on the inner and middle shelf (bottom depth < 50 m), with much lower variability observed on the outer shelf (bottom depth > 50 m) (Fig. 2). The highest physical and biogeochemical variations were observed in the Mississippi plume during 8-11 April and in the Atchafalaya coastal region during 15-17 April (Fig. 3). In spring when river discharge is high and the wind is typically downwelling-favourable, the Mississippi River freshwater generally flows westward in a contained nearshore current (Zhang et al., 2012; Lehrter et al., 2013). Our three end-member mixing model accurately reproduced the westward extension of the Mississippi freshwater on the Louisiana shelf from the Mississippi bird's foot delta (Fig. 2b and Fig. 4a). The mixing model also suggested a westward Atchafalaya plume trajectory in a narrow band along the coast with little Atchafalaya freshwater was transported upcoast toward the Mississippi Delta (Fig. 4b). The pattern of the Mississippi and Atchafalaya freshwater transport agreed well with the multiple-year average condition (2005-2010) in April by hydrodynamic numerical simulation

(Zhang et al., 2012). To better investigate the variability of surface water parameters, we divided the coastal region into four sub-regions: 1) the lower Mississippi River channel (Fig. S2, salinity < 2); 2) the Mississippi plume (Fig. 4a, east of 90.75° W, north of 28.30° N); 3) the high-turbidity Atchafalaya coastal water (Fig. 4a and Fig. 2d, 90.75-92.35° W, light transmittance < 20 %, named as HTACW hereafter); and 4) the Atchafalaya plume (Fig. 4b, 92.35-93.50° W, north of 29.00°

5   N). Typical vertical CTD profiles are shown in the supplement (Figs. S2-S4) to demonstrate the different mixing conditions observed in the four sub-regions as well as other regions in the nGOM.

3.2 Estimates of NCP

In comparison to the discrete measurements of $NCP_{DO-incub}$, $NCP_{\Delta DIC}$, and $NCP_{\Delta NOx}$, the underway O_2/Ar measurements provided NCP_{O2Ar} estimates with the highest resolution and most complete spatial coverage (Fig. 5). The $NCP_{DO-incub}$,

10   $NCP_{\Delta DIC}$, and $NCP_{\Delta NOx}$ were mostly obtained at salinities higher than 20, while the NCP_{O2Ar} covered the whole salinity range (0 to 36.4) providing more information on the NCP variability in the dynamic estuary environments. All methods suggested high variability of NCP in the surface water of the nGOM (Fig. 3c, Fig. 5) and these methods yielded similar spatial patterns with high production rates in the plume region around the Mississippi bird's foot delta (Fig. 5). The results of $NCP_{\Delta DIC}$ (-19.0 to 274.9 mmol C m^{-2} d^{-1}) and $NCP_{\Delta NOx}$ (1.6 to 314.0 mmol C m^{-2} d^{-1}) were close to each other (Fig. 5c, d), and their ranges

15   were similar to that of NCP_{O2Ar} in the Mississippi plume (-99.6 to 235.4 mmol C m^{-2} d^{-1}) (Fig. 3c). $NCP_{DO-incub}$ (-56.0 to 360.7 mmol C m^{-2} d^{-1}) gave the highest NCP estimates in the Mississippi plume (stations C10, A7, and X3 in Fig. 5b and Fig. 3c). As NCP_{O2Ar} is a backward exponentially weighted average rate (Teeter et al., 2018), it is less able to capture high NCP values due to the inherent averaging of the O_2/Ar approach. Moreover, NCP_{O2Ar} could be a poor estimate of daily production rate (e.g., $NCP_{DO-incub}$ in our study) when the mixed layer is not at steady state (Teeter et al., 2018). These could

20   partly explain the observed difference between NCP_{O2Ar} and $NCP_{DO-incub}$ in the dynamic Mississippi plume. In the high-salinity offshore waters, NCP_{O2Ar} and $NCP_{DO-incub}$ both suggest low NCP rates close to zero (Fig. 5a, b). One major difference between NCP_{O2Ar} and $NCP_{DO-incub}$ is that the O_2/Ar method generated negative NCP estimates in the lower Mississippi River channel and in the HTACW while $NCP_{DO-incub}$ suggested positive NCP rates in these regions (Fig. 5a, b).

3.3 Mississippi River channel and plume

Vertical CTD profiles showed strong surface stratification in the lower Mississippi River channel (Fig. S2). The light transmittance in the surface water of the river channel was close to zero (Fig. 6a) and the Chl-a concentrations were low (Fig. 6b) despite ample nutrient availability (NO_x up to 123.3 µmol/kg, Table 1). Similar to most inner estuaries (Borges and Abril, 2011; Chen et al., 2012; Chen and Swaney, 2012), high pCO_2 (up to 1803.0 µatm, Fig. 6c), undersaturated DO (83.7±0.8 %, Fig. 6d) and net CO_2 efflux (55.5±7.6 mmol C m^{-2} d^{-1}, Fig. 6e) was observed in the lower Mississippi River channel. The negative NCP_{O2Ar} (-51.3±11.9 mmol C m^{-2} d^{-1}, Fig. 6f) suggested net heterotrophic condition in the Mississippi River channel which contrasts with the positive $NCP_{DO\text{-}incub}$ (94.5±11.6 mmol C m^{-2} d^{-1} Fig. 7c) measured by the DO incubation method. The Mississippi plume and most offshore regions were characterized by surface stratification, which was mainly caused by the buoyancy of fresher surface water in the plume and vertical temperature gradient in the offshore region (Fig. S3). With increasing light transmittance (Fig. 6a) in conjunction with persistence of riverine-derived nutrient concentrations (Fig. 7a) along the Mississippi plume flow path, phytoplankton biomass reached high levels at intermediate salinities of 15-30 (Fig. 6b). High Chl-a concentrations in the plume region corresponded to large decreases in pCO_2 (down to 113.9 µatm, Fig. 6c) and strong oceanic CO_2 uptake (up to -42.7 mmol m^{-2} d^{-1}, Fig. 6e), as well as elevated DO% (up to 180.1 %, Fig. 6d) and NCP rates (Fig. 6f). The observed high NCP rates (e.g., up to 235.4 mmol C m^{-2} d^{-1} in NCP_{O2Ar}, up to 360.7 mmol C m^{-2} d^{-1} in $NCP_{DO\text{-}incub}$, Fig. 7c) are within the range of prior estimates for this region during spring season (-238 to 624 mmol C m^{-2} d^{-1}, Cai, 2003; Guo et al., 2012; Huang et al., 2012; Lohrenz et al., 1990; 1997; 1999), and are among the highest in large river estuarine and shelf waters (Cooley and Yager, 2006; Dagg et al., 2004; Ning et al., 1988; Ternon et al., 2000).

3.4 Atchafalaya plume and HTACW

The Atchafalaya River discharges in a shallow broad, low-gradient shelf (10 m isobath doesn't occur until more than 40 km offshore of the delta, Fig. 1) which frequently experiences cross-shelf currents (Roberts and Doty, 2015). The Atchafalaya plume water, extended westward in a narrow band along the coast (Fig. 4b) and generally showed similar biogeochemical variability to that observed in the Mississippi plume (Fig. 6). Elevated Chl-a, DO%, and NCP_{O2Ar} were also observed at intermediate salinities o(15-30) in the Atchafalaya plume which also exhibited decreases in pCO_2 and oceanic CO_2 uptake (Fig. 6). For both the Mississippi and Atchafalaya plume regions, the three end-member mixing model suggests that the

enhanced biological production resulted in significant deviations of DIC and NO_x from the conservative mixing lines (Fig. 8). The amplitudes of the non-conservative biological removal of nutrients (up to 35 μmol kg^{-1} in ΔNO_{xNCP}, Fig. 8a) and DIC (up to 250 μmol kg^{-1} in ΔDIC_{NCP}, Fig. 8b) are similar to the findings of previous studies in the nGOM (Cai, 2003; Guo et al., 2012; Huang et al., 2012). The biological uptake ratio of ΔNO_{xNCP} and ΔDIC_{NCP} (0.14 in Fig. 8c) was close to the Redfield

5   N:C ratio (16:106 = 0.15). However, NCP_{O2Ar} suggested that the southwest part of the Atchafalaya plume (around 29.30° N, 93.50° W) was heterotrophic (Fig. 5a). A detailed examination of the CTD profiles revealed that the water column in this area was vertically well-mixed (Fig. S4), which was different than the stratification observed in other plume regions. The HTACW was characterized by a well-mixed water column and low light transmittance (Fig. S4). Although the Chl-a concentrations in the HTACW were similar to those in the Atchafalaya plume in the salinity range of 24 to 32 (Fig. 6b), the

10   DO% was much lower in the HTACW (94.7±12.1 %, Fig. 6d). The pCO_2 in the HTACW (327.8±34.6 μatm) was higher than that in the Atchafalaya plume (288.7±43.7 μatm) at the same salinities (Fig. 6c), but the HTACW still acted as a weak sink for atmospheric CO_2 (-7.1±3.1 mmol C m^{-2} d^{-1}, Fig. 6e). Similar to that in the Mississippi River channel, the two approaches for NCP estimation presented contrasting results in the HTACW: negative NCP_{O2Ar} (-39.2±14.0 mmol C m^{-2} d^{-1}, Fig. 5a) suggest net heterotrophic conditions while positive $NCP_{DO\text{-}incub}$ rates (62.6±23.3 mmol C m^{-2} d^{-1}, Fig. 5b) suggest net

15   autotrophic conditions.

4. Discussion

4.1 Comparison of NCP estimations

A comparison of NCP estimated from various methods should be interpreted with caution as each approach has its independent assumptions and limitations and refers to different temporal and spatial scales (Ulfsbo et al., 2014). However,

20   applying multiple methods provides complementary information to better understand the processes affecting estimations of and controls on ecosystem metabolism.

NCP from the DO incubation method: The $NCP_{DO\text{-}incub}$ was estimated from 24-hour DO changes in incubation bottles, which gives a daily NCP estimate for the plankton community at the sampling location. The DO incubation method is a direct measurement of NCP and is free from the influences of lateral advection and sediment metabolism. $NCP_{DO\text{-}incub}$ thus equals

the MLD-integrated NCP in the stratified regions (NCP_{MLD} in Fig. 9a, c) or the water column-integrated NCP in the well-mixed regions (NCP_{water} in Fig. 9b). However, there are uncertainties related to scaling from samples collected at discrete depths to integrated mixed layer NCP values. First, the scaling method used here assumes a homogenous distribution of respiration rate over the MLD. Second, we only measured GPP at one light level (50 %) and we assumed that the GPP below

5   50 % surface PAR was linearly scaled to %PAR (Eq. 6 and Eq. 7). Similar assumptions for the Louisiana shelf were tested previously by Murrell and Lehrter, (2011) who found that single point measurements (vs. multi-point measurements in a layer) provided robust estimates of integrated rates. However, in the current study, the assumption has been further applied to shallow nearshore sites (< 10 m depth), which may exhibit greater heterogeneity in vertical PAR distributions due to the high algal biomass and suspended sediment particle concentrations. More importantly, for high-turbidity water samples (e.g.,

10   samples collected in the Mississippi River channel and in the HTACW), the incubated samples were not mixed in the same way as that in the natural environment and the sedimentation of particles in incubation bottles could alleviate the light limitation for phytoplankton. As a result, the gross primary production (GPP_{Int} in Eq. 8) could be overestimated and $NCP_{DO\text{-}incub}$ would not represent the true *in situ* NCP in high-turbidity waters.

NCP from the O_2/Ar method: NCP_{O2Ar} is derived from the air-sea biological oxygen flux (Eq. 4), which represents the

15   exponentially weighted NCP over the past several residence times of O_2 (Kaiser et al. 2005; Teeter et al. 2018). When using the O_2/Ar method to estimate NCP_{MLD}, a key assumption is that physical inputs to the mixed layer are negligible. However, this assumption can be invalid in the dynamic coastal environments. Recent studies have shown that entrainment and upwelling processes (mixing with O_2-depleted subsurface water) can lead to significant underestimation in NCP_{MLD} using the O_2/Ar method, especially in coastal upwelling zones (Castro-Morales et al., 2013; Nicholson et al., 2012; Shadwick et al.,

20   2015; Teeter et al., 2018). As most regions in our study were characterized by the persistent surface stratification (Figs. S2 and S3), the influences of sub-pycnocline ($NCP_{sub\text{-}MLD}$ in Fig. 9a, c) and benthic metabolisms ($NCP_{benthic}$ in Fig. 9a, c) on the surface O_2/Ar ratio were expected to be minor. However, the surface O_2/Ar ratio in the well-mixed nearshore regions (e.g., the HTACW, Fig. S4) was affected by both water column (NCP_{water}) and benthic metabolisms ($NCP_{benthic}$) (Fig. 9b). Moreover, both Mississippi and Atchafalaya river end-members were highly heterotrophic and lateral transportation of this

25   heterotrophic signal carried by river water (NCP_{adv} in Fig. 9) should be considered. As it generally takes a few days for O_2 to

14

become in equilibrium with the atmosphere (see the discussion below), NCP_{adv} could play an important role affecting the O_2/Ar ratio in the river channel and estuary where water transport speed was rapid (Fig. 9a, b). The influence of NCP_{adv} decreased offshore and the impact of remote source water heterotrophy was negligible in most offshore regions where water residence time was sufficiently long (Fig. 9c). Therefore, NCP_{O2Ar} represented the metabolic state of the water which was

5   affected not only by the local aquatic ecosystem (NCP_{MLD} or NCP_{water} in Fig. 9), but also by additional factors including $NCP_{benthic}$ and NCP_{adv} (Fig. 9). Depending on the different mixing conditions in the nGOM, NCP_{O2Ar} reflected either 1) the combined result of NCP_{MLD} and NCP_{adv} in the stratified river channel and plume region; 2) the combined result of NCP_{water}, $NCP_{benthic}$, and NCP_{adv} in the well-mixed nearshore waters (e.g., HTACW); or 3) NCP_{MLD} in the offshore stratified regions where riverine influence was minor. As $NCP_{benthic}$ only affected a small portion of the nearshore water in the Atchafalaya

10   coastal region (Fig. S4), the NCP_{O2Ar} measured in this study was mainly modulated by NCP_{MLD} and NCP_{adv}. Considering the nGOM as a whole, lateral advection of NCP_{adv} can be considered as internal transport within the system given that the NCP_{O2Ar} was measured with adequate spatial coverage. As a result, the NCP_{O2Ar} measured in this study well represented the overall metabolic state of the surface water of the nGOM.

NCP from the non-conservative changes in DIC and nutrients: The $NCP_{\Delta DIC}$ and $NCP_{\Delta NOx}$ in the Mississippi plume reflected

15   the average community production rate along the flow path during the river-ocean mixing process. There are several sources of uncertainty associated with the NCP estimated from the non-conservative mixing change in DIC and nutrients. First, errors in estimating water residence time and the changes in MLD over the transit time of the plume water lead to proportional errors in the calculation of $NCP_{\Delta DIC}$ and $NCP_{\Delta NOx}$ (Eq. 13 and Eq. 14). The plume water residence time is a function of river discharge and other physical conditions, it is therefore expected that using a set of past model-assessed τ

20   values probably would introduce the largest uncertainty in the estimation of $NCP_{\Delta DIC}$ and $NCP_{\Delta NOx}$. Second, uncertainty may be caused by the changes in the concentrations of DIC and nutrients of the river end-members. However, this uncertainty decreases with salinity (Huang et al., 2012) and was generally low in our study.

To better investigate the NCP rates estimated from different methods, we focused on the regions where NCP_{O2Ar} and $NCP_{DO-incub}$ provided contrasting results: NCP_{O2Ar} suggested heterotrophy in the Mississippi River channel and in the HTACW where

25   positive $NCP_{DO-incub}$ rates were presented. The contrasting results of NCP_{O2Ar} and $NCP_{DO-incub}$ can be mainly explained by the

different spatial and temporal scales associated with the two methods responding to the mixing conditions. In the high-turbidity Mississippi River channel (light transmittance close to zero) and HTACW (light transmittance <20 %), the GPP was strongly limited by light availability and the DO incubation method could significantly overestimate the *in situ* NCP due to the improved light environment in the incubation bottles. However, the measured community respiration rates ($Resp_{Int}$ in Eq. 8) in the lower

5 Mississippi River channel (14.0±0.8 mmol C m^{-2} d^{-1}) and in the HTACW (30.5±10.7 mmol C m^{-2} d^{-1}) were not able to fully account for the heterotrophy suggested by NCP_{O2Ar} (-51.3±11.9 and -39.2±14.0 mmol C m^{-2} d^{-1} in the lower Mississippi River channel and HTACW respectively) even when the GPP was not taken into account. This indicates sources of heterotrophic signal other than the local community respiration in these two regions. In the stratified lower Mississippi River channel (Fig. 9a), the influence of lateral transportation of the heterotrophic river water from the upper river channel was significant because

10 of the short water residence time (~1 day, Green et al., 2006). The heterotrophic condition in the lower Mississippi River channel could be attributed to the dominant influence of the heterotrophic NCP_{adv} over the local biological production. In the vertically well-mixed HTACW (Fig. 9b), NCP_{O2Ar} reflected the combined result of the water column community production, the lateral advection of CO_2-rich Atchafalaya river water (NCP_{adv}), and sediment metabolism ($NCP_{benthic}$). High sediment oxygen consumption and bottom water community respiration rates were observed in the Atchafalaya River Delta Estuary

15 (Roberts and Doty, 2015) and on the Louisiana continental shelf (Murrell and Lehrter, 2011; Murrell et al., 2013). These studies suggested that the total below-pycnocline respiration rates show low variability over a large geographic and temporal range in the nGOM (46.4 to 104.5 mmol O$_2$ m^{-2} d^{-1}). The negative NCP_{O2Ar} observed in the HTACW by our study (-39.2±14.0 mmol C m^{-2} d^{-1}) agreed with the finding of Murrell et al. (2013) which showed shelf-scale net water column heterotrophy on the Louisiana shelf. This water column heterotrophy can be well explained by the combined results of NCP_{water}, $NCP_{benthic}$ and

20 NCP_{adv}. The same logic can be applied to explain the net heterotrophy observed in the southwest part of the Atchafalaya plume with well-mixed water column (negative NCP_{O2Ar} around 29.30° N, 93.50° W, Fig. 5a).

4.2 Controls on the surface NCP and CO_2 flux

As the underway O_2/Ar method provided the highest resolution NCP estimation coupled with pCO$_2$ measurement, NCP_{O2Ar}

25 was presented together with the CO_2 variables in the following sections to investigate the variability and controls on the

16

metabolic balance of the system. Nutrients, irradiance, and mixing were considered to be the major controlling factors of biological production in coastal waters of the nGOM (Lehrter et al., 2009; Lohrenz et al., 1999; Murrell et al., 2013; Turner and Rabalais, 2013). Here we use the results in the Mississippi plume (data averaged over increments of two salinity units, Fig. 7) to demonstrate the controlling mechanisms of the changes in surface NCP and CO_2 flux with the increasing salinity. There is an ecological gradient along the river-ocean mixing continuum: from turbid, eutrophic freshwater to clear, oligotrophic offshore oceanic waters (Fig. 7a). The freshwater input from the Mississippi River was characterized by strong heterotrophy with high DIC and pCO_2 supported by the decomposition of terrestrial organic carbon (Bianchi et al., 2010). Meanwhile, phytoplankton growth and production were limited by light availability in the high-turbidity Mississippi River channel despite the high nutrient concentration (Fig. 7a-c). The net heterotrophy of the water at the low salinity end and the corresponding CO_2 outgassing (Fig. 7d) were attributed to the terrestrial carbon input, light limitation on primary production, and short water residence time (Lehrter et al., 2009; Lohrenz et al., 1990; 1999; Roberts and Doty, 2015). While high CO_2 efflux was observed at low salinities, its contribution to the overall regional CO_2 flux was relatively small due to the limited spatial coverage of low salinity regions (Huang et al., 2015).

Due to the alleviation of light limitation in conjunction with persistence of riverine nutrient concentrations, Chl-a, DO% and NCP_{O2Ar} all showed an increasing trend with salinity along the flow path of the Mississippi plume (Fig. 8). A positive correlation between the mean NCP_{O2Ar} rates and Chl-a concentrations (Fig. 7b, d) was observed in the Mississippi plume (r^2 = 0.75, figure not shown) where light availability generally determined the onset of the biological growth and the river-borne nutrient loading set the magnitude of biological production (Fig. 7, Fig. 8). At intermediate salinities (15 to 30) in the Mississippi plume, there existed an "optimal growth region" where light and nutrient availability were both favourable for phytoplankton growth (Fig. 7) (Cloern et al., 2013; Demaster et al., 1996; Seguro et al., 2015). High NCP_{O2Ar} (114.8±54.6 mmol C m^{-2} d^{-1}) was observed in this optimal growth region corresponding to an oceanic CO_2 uptake of -13.5±5.3 mmol C m^{-2} d^{-1} (Fig. 7d). In high-salinity offshore water, phytoplankton growth and production were primarily limited by depleted nutrient concentration (Lehrter et al. 2009; Lohrenz et al. 1990; Lohrenz et al. 1999). Because of the minor terrestrial influence and low biological production, DO and pCO_2 in the offshore gulf water were close to equilibrium with atmosphere and NCP_{O2Ar} and CO_2 flux were close to zero (Fig. 7).

The spatial variability of NCP and CO_2 flux in the nGOM are associated with the trajectory of the Mississippi and Atchafalaya plume as the surface biogeochemical variations are strongly affected by riverine influences. For instance, an unusually broad plume extension in the nGOM in March 2010, driven by upwelling favourable wind and high freshwater discharge, was associated with elevated chlorophyll concentrations and stronger biological CO_2 uptake (Huang et al., 2013). Modeling studies

5   also suggest that NCP and CO_2 fluxes in the nGOM are susceptible to changes in river and wind forcing (Fennel et al., 2011; Xue et al., 2016). To better study the variability of surface NCP and CO_2 flux, further studies are needed to investigate how the seasonal and inter-annual variations in environmental conditions (freshwater discharge, riverine inputs of carbon and nutrients, wind forcing, coastal circulation etc.) affect the trajectory of the river plume and the biological processes therein.

4.3 Coupling between NCP and CO_2 flux

10   Overall, the surface water of the nGOM (93.00-89.25° W, 28.50-29.50° N) was estimated to be net autotrophic during our study period with an area-weighted mean NCP_{O2Ar} rate of 21.2 mmol C m^{-2} d^{-1} and as a CO_2 sink of -6.7 mmol C m^{-2} d^{-1}. When plotting the paired CO_2 flux and NCP_{O2Ar} data (Fig. 10), most data collected in the lower Mississippi River channel fall in quadrant 2 suggesting net heterotrophy coupled with CO_2 outgassing to the atmosphere. The Mississippi plume and Atchafalaya plume exhibited opposite patterns with most data in these regions being in quadrant 4 (net autotrophy coupled

15   with CO_2 uptake from the atmosphere). However, the data in quadrant 1 (autotropic water as a CO_2 source observed near the Mississippi River mouth) and quadrant 3 (heterotopic water as a CO_2 sink in the HTACW) suggest decoupling between NCP_{O2Ar} and CO_2 flux.

Here we use the box model (Section 2.5) to investigate the relationship between NCP and air-sea gas fluxes of O_2 and CO_2. We calculated the re-equilibrium time for O_2 and CO_2 following the occurrence of 10 days biological modification: NCP was

20   set as 50 (net autotrophy) or -50 (net heterotrophy) mmol C m^{-2} d^{-1} from days 0 to 10, and as zero after day 11 (Fig. S5). The air-sea O_2 flux rapidly reached a balance with the NCP-induced O_2 changes for both the autotrophy and heterotrophy simulations with the re-equilibrium time for O_2 for each estimation to be a few days (Fig. S5). Given the same environmental settings, the re-equilibrium time for CO_2 was much longer (more than one month, Fig. S5). This is related to the relative slow air-sea CO_2 exchange rate, and, more importantly the carbonate buffering system, i.e., the gas exchange-induced

25   changes in aquatic CO_2 are buffered by a much larger carbon pool of $HCO_3^- $-$CO_3^{2-}$ (Zeebe and Wolf-Gladrow, 2001).

NCP affects air-sea gas exchange of CO_2 through its influence on pCO_2 in the surface water. Net autotrophy results in a net biological uptake of CO_2 from the seawater (decrease in $\Delta pCO_{2(sea-air)}$ in Eq. 1) while net heterotrophy has the opposite effect. However, $\Delta pCO_{2(sea-air)}$ is not only affected by *in situ* NCP (ΔpCO_{2NCP}), but also by the background level of ΔpCO_2 which is related to the preceding mixing and biological processes ($\Delta pCO_{2background}$): $\Delta pCO_{2(sea-air)} = \Delta pCO_{2background} + \Delta pCO_{2NCP}$.

5   Therefore, local ecosystem net autotrophy (negative ΔpCO_{2NCP}) does not necessarily result in CO_2 uptake from the atmosphere (negative $\Delta pCO_{2(sea-air)}$) if the NCP-induced pCO_2 decrease occurs in a water with high heterotrophic background (highly positive $\Delta pCO_{2background}$). Similarly, net heterotrophy does not necessarily result in a CO_2 outgassing if the source water is highly autotrophic.

In the simulation with time-dependent varying NCP rates (Fig. 11), we demonstrated how the preceding biological processes

10   and the lingering background pCO_2 affect the relationship between NCP and CO_2 flux. The NCP rate in this simulation was set as 0 during days 0 to 30, changed to -50 mmol C m^{-2} d^{-1} (net heterotrophy) during days 31 to 60, then to 100 mmol C m^{-2} d^{-1} (net autotrophy) during days 61 to 90, and to -50 mmol C m^{-2} d^{-1} again during days 91 to 120 (Fig. 11a). Although NCP changed instantly, the backward exponentially weighted NCP derived from the bioflux of O_2 (NCP_{O2Ar} in Fig. 11a) lagged a few days behind NCP. After each change in NCP, the memory effect of the preceding NCP on DO was small as the air-sea

15   O_2 exchange quickly balanced the NCP-induced O_2 production or consumption within several days (Fig. 11b, c). In contrast, the slow CO_2 gas exchange and long re-equilibrium time of CO_2 generated a significant memory effect of the preceding NCP on $\Delta pCO_{2(sea-air)}$ (Fig. 11b, c). The combined result of *in situ* production and the lingering effect of background pCO_2 thus resulted in the decoupling between NCP_{O2Ar} and CO_2 flux (data in quadrant 1 and quadrant 3 in Fig. 11d). One typical example is the results during days 91 to 120 (data in quadrant 3 in Fig. 11d): the strong preceding autotrophic production

20   during days 61 to 90 led to highly negative $\Delta pCO_{2background}$ (-315.5 μatm on day 90, Fig. 11c), which resulted in the water acting as a CO_2 sink during days 91 to 120 (Fig. 11b) although the *in situ* heterotrophic NCP increased pCO_2 during this time period (Fig. 11c).

In summary, the decoupling between NCP and CO_2 flux can be the result of competing effect of $\Delta pCO_{2background}$ and ΔpCO_{2NEP}. In our observations, surface waters with oversaturated pCO_2 and positive NCP_{O2Ar} (data in quadrant 1 in Fig. 10)

25   were observed directly outside of the Mississippi River mouth. This is the region where *in situ* autotrophic biological

productivity began to increase due to alleviated light limitation, but the highly heterotrophic $\Delta p\text{CO}_{2\text{background}}$ from the river channel resulted in the water in this region still acting as a CO_2 source. Decoupling was also observed in the HTACW where CO_2 uptake occurred under heterotrophic condition (data in quadrant 3 in Fig. 10). As discussed above, this phenomenon can be explained by *in situ* heterotrophy superimposed on surface water with low background $p\text{CO}_2$ resulting from the preceding autotrophic biological production.

Conclusions

During a spring cruise in the northern Gulf of Mexico in April 2017, we found encouraging agreement among NCP estimates from multiple approaches despite the different temporal and spatial resolutions and uncertainties associated with each approach. Our study showed that the DO incubation approach represents the daily NCP by the local plankton community while the O_2/Ar method reflects the metabolic state of the water relating to both biological and physical processes over longer time scales. The DO incubation method may significantly overestimate NCP rates for high-turbidity water samples due to the improved light environment in the incubation bottles. The O_2/Ar method has the advantage of being able to provide high-resolution NCP estimates matching the underway $p\text{CO}_2$ measurement, which provides more accurate estimation of the overall metabolic condition of the surface water of the nGOM and also allows a better examination on the NCP and CO_2 dynamics. The NCP_{O2Ar} and CO_2 flux showed higher spatial variability on the inner and middle shelf which was strongly influenced by the Mississippi-Atchafalaya River system. Along the river-ocean mixing gradient, NCP_{O2Ar} and CO_2 flux were characterized by 1) heterotrophy and CO_2 release at low salinities resulting from the decomposition of terrestrial carbon and light limitation on photosynthesis, 2) strong autotrophy and CO_2 uptake at intermediate salinities of 15-30 where light and nutrient are both favourable for phytoplankton growth, 3) close-to-zero NCP rate and CO_2 flux in the offshore seawater resulting from nutrient limitation. This study also demonstrated that, due to the slow air-sea CO_2 exchange and the buffering effect of the carbonate system, decoupling between NCP and CO_2 flux could be observed as the competing result of *in situ* biological production and the lingering effect of background $p\text{CO}_2$ of the source water.

20

Data availability.

Data of this study are available from the Biological and Chemical Oceanography Data Management Office: https://www.bco-dmo.org/project/751332.

Author contributions

5   Z-P.J., J.L., B.C., Z.O., N.H., M.K.S., and J.Z attended the nGOM cruise and all authors contributed to the data collection: O_2/Ar (Z-P.J., Z.O), incubation experiments (J.L.), pCO$_2$ (B.C.), DO (N.H.), DIC and TA (M.K.S., J.Z., Y.X.), nutrient (B.J.R.), and model and remote sensing (C.L.). W-J.C. designed and led the whole project. W-J.C. is the PI who supervised the sample analysis, data analysis and writing. Z-P.J. is the primary author while all co-authors were involved in discussion and writing by providing comments.

10   **Competing interests.**

The authors declare that they have no conflict of interest.

Acknowledgement

References

20   Álvarez, M., H. Sanleón-Bartolomé, T. Tanhua, L. Mintrop, A. Luchetta, C. Cantoni, K. Schroeder, and G. Civitarese. The CO$_2$ system in the Mediterranean Sea: a basin wide perspective, Ocean Science, **10**(1), 69-92. 2014.

Bauer, J. E., W. J. Cai, P. A. Raymond, T. S. Bianchi, C. S. Hopkinson, and P. a. G. Regnier. The changing carbon cycle of the coastal ocean. Nature **504:** 61-70. 2013.

Bianchi, T. S., S. F. Dimarco, J. H. Cowan, R. D. Hetland, P. Chapman, J. W. Day, and M. A. Allison. The science of hypoxia

in the Northern Gulf of Mexico: A review. Science of the Total Environment **408:** 1471-1484. 2010.

Borges, A. V., and G. Abril. Carbon dioxide and methane dynamics in estuaries, p. 119-161. Treatise on estuarine and coastal science. Academic Press. 2011.

Brewer, P. G., and J. C. Goldman. Alkalinity changes generated by phytoplankton growth. Limnology and Oceanography **21:** 108-117. 1976.

Cai, W. J. Riverine inorganic carbon flux and rate of biological uptake in the Mississippi River plume. Geophysical Research Letters **30**(2). 2003.

Cai, W. J. Estuarine and coastal ocean carbon paradox: CO_2 sinks or sites of terrestrial carbon incineration? Annual Review of Marine Science, **3:** 123-145. 2011.

Cai, W. J., M. H. Dai, and Y. C. Wang. Air-sea exchange of carbon dioxide in ocean margins: A province-based synthesis, Geophysical Research Letters **33:** L12603. 2006.

Cai, W. J., X. P. Hu, W. J. Huang, M. C. Murrell, J. C. Lehrter, S. E. Lohrenz, W. C. Chou, W. D. Zhai, J. T. Hollibaugh, Y. C. Wang, P. S. Zhao, X. H. Guo, K. Gundersen, M. H. Dai, and G. C. Gong. Acidification of subsurface coastal waters enhanced by eutrophication. Nature Geoscience **4:** 766-770. 2011.

Cassar, N., B. A. Barnett, M. L. Bender, J. Kaiser, R. C. Hamme, and B. Tilbrook. Continuous high-frequency dissolved O_2/Ar measurements by equilibrator inlet mass spectrometry. Analytical Chemistry **81:** 1855-1864. 2009.

Cassar, N., P. J. Difiore, B. A. Barnett, M. L. Bender, A. R. Bowie, B. Tilbrook, K. Petrou, K. J. Westwood, S. W. Wright, and D. Lefevre. The influence of iron and light on net community production in the Subantarctic and Polar Frontal Zones. Biogeosciences **8:** 227-237. 2011.

Cloern, J.E., Jassby, A.D., Patterns and scales of phytoplankton variability in estuarine-coastal ecosystems. Estuaries Coasts **33**, 230–241. 2010.

Castro-Morales, K., N. Cassar, D. R. Shoosmith, and J. Kaiser. Biological production in the Bellingshausen Sea from oxygen-to-argon ratios and oxygen triple isotopes. Biogeosciences **10:** 2273-2291. 2013.

Chen, C.-T. A., and A. V. Borges. Reconciling opposing views on carbon cycling in the coastal ocean: Continental shelves as sinks and near-shore ecosystems as sources of atmospheric CO_2. Deep-Sea Research Part II-Topical Studies in Oceanography **56:** 578-590. 2009.

Chen, C.-T. A., T.-H. Huang, Y.-H. Fu, Y. Bai, and X. He. Strong sources of CO_2 in upper estuaries become sinks of CO_2 in large river plumes. Current Opinion in Environmental Sustainability **4:** 179-185. 2012.

Chen, C. T. A., and D. P. Swaney. Terrestrial-ocean transfers of carbon and nutrient across the coastal boundary: Editorial overview. Current Opinion in Environmental Sustainability **4:** 159-161. 2012.

Chen, X., S. E. Lohrenz, and D. A. Wiesenburg. Distribution and controlling mechanisms of primary production on the Louisiana–Texas continental shelf. Journal of Marine Systems **25:** 179-207. 2000.

Cooley, S. R., and P. L. Yager. Physical and biological contributions to the western tropical North Atlantic Ocean carbon sink formed by the Amazon River plume. Journal of Geophysical Research-Oceans **111**. 2006.

Craig, H., and T. Hayward. Oxygen supersaturation in the ocean: Biological versus physical contributions. Science **235:** 199-202. 1987.

Dagg, M., R. Benner, S. Lohrenz, and D. Lawrence. Transformation of dissolved and particulate materials on continental shelves influenced by large rivers: plume processes. Continental Shelf Research **24:** 833-858. 2004.

5   Demaster, D. J., W. O. Smith, D. M. Nelson, and J. Y. Aller. Biogeochemical processes in Amazon shelf waters: Chemical distributions and uptake rates of silicon, carbon and nitrogen. Continental Shelf Research **16:** 617-643. 1996.

Diaz, R. J., and R. Rosenberg. Spreading dead zones and consequences for marine ecosystems. Science **321:** 926-929. 2008.

Dickson, A. G., C. L. Sabine, and J. R. Christian. Guide to best practices for ocean CO_2 measurements. North Pacific Marine Science Organization (PICES). 2007.

10   Egleston, E. S., C. L. Sabine, and F. M. M. Morel. Revelle revisited: Buffer factors that quantify the response of ocean chemistry to changes in DIC and alkalinity, Global Biogeochemical Cycles, **24**. 2010.

Eppley, R. W., and B. J. Peterson. Particulate organic matter flux and planktonic new production in the deep ocean. Nature **282:** 677-680. 1979.

Fennel, K., R. Hetland, Y. Feng, and S. Dimarco. A coupled physical-biological model of the Northern Gulf of Mexico shelf: model description, validation and analysis of phytoplankton variability. Biogeosciences **8:** 1881-1899. 2011.

15

Garcia, H. E., and L. I. Gordon. Oxygen solubility in seawater: Better fitting equations. Limnology and Oceanography **37:** 1307-1312. 1992.

Gattuso, J.-P., M. Frankignoulle, and R. Wollast. Carbon and carbonate metabolism in coastal aquatic ecosystems. Annual Review of Ecology, Evolution, and Systematics **29:** 405-434. 1998.

20   Geider, R. J., and J. La Roche. Redfield revisited: variability of C:N:P in marine microalgae and its biochemical basis. European Journal of Phycology **37:** 1-17. 2002.

Green, R. E., T. S. Bianchi, M. J. Dagg, N. D. Walker, and G. A. Breed. An organic carbon budget for the Mississippi River turbidity plume and plume contributions to air-sea CO_2 fluxes and bottom water hypoxia. Estuaries and Coasts **29:** 579-597. 2006.

25   Guo, X., W.-J. Cai, W.-J. Huang, Y. Wang, F. Chen, M. C. Murrell, S. E. Lohrenz, L.-Q. Jiang, M. Dai, J. Hartmann, Q. Lin, and R. Culp. Carbon dynamics and community production in the Mississippi River plume. Limnology and Oceanography **57:** 1-17. 2012.

Hamme, R. C., and S. R. Emerson. The solubility of neon, nitrogen and argon in distilled water and seawater. Deep-Sea Research Part I-Oceanographic Research Papers **51:** 1517-1528. 2004.

30   Hodur, R. M. The Naval Research Laboratory's coupled ocean/Atmosphere Mesoscale Prediction System (COAMPS). Monthly Weather Review **125:** 1414-1430. 1997.

Huang, W. J., W. J. Cai, R. M. Castelao, Y. C. Wang, and S. E. Lohrenz. Effects of a wind-driven cross-shelf large river plume on biological production and CO_2 uptake on the Gulf of Mexico during spring. Limnology and Oceanography **58:** 1727-1735. 2013.

Huang, W. J., W. J. Cai, R. T. Powell, S. E. Lohrenz, Y. Wang, L. Q. Jiang, and C. S. Hopkinson. The stoichiometry of inorganic carbon and nutrient removal in the Mississippi River plume and adjacent continental shelf. Biogeosciences **9**: 2781-2792. 2012.

Huang, W. J., W. J. Cai, Y. C. Wang, S. E. Lohrenz, and M. C. Murrell. The carbon dioxide system on the Mississippi River-dominated continental shelf in the northern Gulf of Mexico: 1. Distribution and air-sea CO_2 flux. Journal of Geophysical Research-Oceans **120**: 1429-1445. 2015.

Jonsson, B. F., S. C. Doney, J. Dunne, and M. Bender. Evaluation of the Southern Ocean O_2/Ar-based NCP estimates in a model framework. Journal of Geophysical Research-Biogeosciences **118**: 385-399. 2013.

Justić, D., N. N. Rabalais, R. Eugene Turner, and W. J. Wiseman. Seasonal coupling between riverborne nutrients, net productivity and hypoxia. Marine Pollution Bulletin **26**: 184-189. 1993.

Kaiser, J., M. K. Reuer, B. Barnett, and M. L. Bender. Marine productivity estimates from continuous O_2/Ar ratio measurements by membrane inlet mass spectrometry. Geophysical Research Letters **32**. 2005.

Laruelle, G. G., H. H. Durr, C. P. Slomp, and A. V. Borges. Evaluation of sinks and sources of CO_2 in the global coastal ocean using a spatially-explicit typology of estuaries and continental shelves. Geophysical Research Letters **37**. 2010.

Laws, E. A. Photosynthetic quotients, new production and net community production in the open ocean. Deep-Sea Research Part a-Oceanographic Research Papers **38**: 143-167. 1991.

Lawson, C. L., and R. J. Hanson. Solving Least Squares Problems. Prentice-Hall, Chapter 23, 161 pp. 1974.

Lehrter, J. C., D. S. Ko, M. C. Murrell, J. D. Hagy, B. A. Schaeffer, R. M. Greene, R. W. Gould, and B. Penta. Nutrient distributions, transports, and budgets on the inner margin of a river-dominated continental shelf, Journal of Geophysical Research: Oceans, **118**(10), 4822-4838. 2013.

Lehrter, J. C., M. C. Murrell, and J. C. Kurtz. Interactions between freshwater input, light, and phytoplankton dynamics on the Louisiana continental shelf. Continental Shelf Research **29**: 1861-1872. 2009.

Lohrenz, S. E., W.-J. Cai, F. Chen, X. Chen, and M. Tuel. Seasonal variability in air-sea fluxes of CO_2 in a river-influenced coastal margin. Journal of Geophysical Research: Oceans **115** (C10). 2010.

Lohrenz, S. E., W. J. Cai, S. Chakraborty, K. Gundersen, and M. C. Murrell. Nutrient and carbon dynamics in a large river-dominated coastal ecosystem: the Mississippi-Atchafalaya River system. Biogeochemical Dynamics at Major River-Coastal Interfaces: Linkages with Global Change**:** 448-472. 2014.

Lohrenz, S. E., M. J. Dagg, and T. E. Whitledge. Enhanced primary production at the plume pceanic interface of the Mississippi River. Continental Shelf Research **10**: 639-664. 1990.

Lohrenz, S. E., G. L. Fahnenstiel, D. G. Redalje, G. A. Lang, X. G. Chen, and M. J. Dagg. Variations in primary production of northern Gulf of Mexico continental shelf waters linked to nutrient inputs from the Mississippi River. Marine Ecology Progress Series **155**: 45-54. 1997.

Lohrenz, S. E., G. L. Fahnenstiel, D. G. Redalje, G. A. Lang, M. J. Dagg, T. E. Whitledge, and Q. Dortch. Nutrients, irradiance, and mixing as factors regulating primary production in coastal waters impacted by the Mississippi River plume.

Continental Shelf Research **19:** 1113-1141. 1999.

Mckee, B. A., R. C. Aller, M. A. Allison, T. S. Bianchi, and G. C. Kineke. Transport and transformation of dissolved and particulate materials on continental margins influenced by major rivers: benthic boundary layer and seabed processes. Continental Shelf Research **24:** 899-926. 2004.

Muller-Karger, F. E., R. Varela, R. Thunell, R. Luerssen, C. M. Hu, and J. J. Walsh. The importance of continental margins in the global carbon cycle, Geophysical Research Letters **32**(1): L01602. 2005.

Murrell, M. C., J. G. Campbell, J. D. Hagy III, and J. M. Caffrey. Effects of irradiance on benthic and water column processes in a Gulf of Mexico estuary: Pensacola Bay, Florida, USA. Estuarine, Coastal and Shelf Science 81: 501–512. 2009.

Murrell, M. C., and J. C. Lehrter, Sediment and lower water column oxygen consumption in the seasonally hypoxic region of the Louisiana Continental Shelf. Estuaries and Coasts, 34, 912-924. 2011.

Murrell, M. C., R. S. Stanley, J. C. Lehrter, and J. D. Hagy. Plankton community respiration, net ecosystem metabolism, and oxygen dynamics on the Louisiana continental shelf: Implications for hypoxia. Continental Shelf Research **52:** 27-38. 2013.

Nicholson, D. P., R. H. R. Stanley, E. Barkan, D. M. Karl, B. Luz, P. D. Quay, and S. C. Doney. Evaluating triple oxygen isotope estimates of gross primary production at the Hawaii Ocean Time-series and Bermuda Atlantic Time-series Study sites. Journal of Geophysical Research-Oceans **117**. 2012.

Ning, X. R., D. Vaulot, Z. S. Liu, and Z. L. Liu. Standing stock and production of phytoplankton in the estuary of the Changjiang (Yangtse River) and the adjacent East China Sea. Marine Ecology Progress Series **49:** 141-150. 1988.

Obenour, D. R., D. Scavia, N. N. Rabalais, R. E. Turner, and A. M. Michalak. Retrospective analysis of midsummer hypoxic area and volume in the Northern Gulf of Mexico, 1985–2011. Environmental Science & Technology **47:** 9808-9815. 2013.

Pai, S.-C., G.-C. Gong, and K.-K. Liu. Determination of dissolved oxygen in seawater by direct spectrophotometry of total iodine. Marine Chemistry **41:** 343-351. 1993.

Pierrot, D., E. Lewis, and D. W. R. Wallace. MS Excel program developed for CO_2 system Calculations, ORNL/CDIAC-105a. Carbon Dioxide Information Analysis Center, Oak Ridge National Laboratory, US Department of Energy, Oak Ridge, TN, doi:10.3334/CDIAC/otg.CO2SYS_XLS_CDIAC105a. 2006.

Rabalais, N. N., W. J. Cai, J. Carstensen, D. J. Conley, B. Fry, X. P. Hu, Z. Quinones-Rivera, R. Rosenberg, C. P. Slomp, R. E. Turner, M. Voss, B. Wissel, and J. Zhang. Eutrophication-driven deoxygenation in the coastal ocean. Oceanography **27:** 172-183. 2014.

Rabalais, N. N., R. E. Turner, and W. J. Wiseman. Gulf of Mexico hypoxia, aka "The dead zone". Annual Review of Ecology and Systematics **33:** 235-263. 2002.

Regnier, P., P. Friedlingstein, P. Ciais, F. T. Mackenzie, N. Gruber, I. A. Janssens, G. G. Laruelle, R. Lauerwald, S. Luyssaert, A. J. Andersson, S. Arndt, C. Arnosti, A. V. Borges, A. W. Dale, A. Gallego-Sala, Y. Godderis, N. Goossens, J. Hartmann, C. Heinze, T. Ilyina, F. Joos, D. E. Larowe, J. Leifeld, F. J. R. Meysman, G. Munhoven, P. A. Raymond,

R. Spahni, P. Suntharalingam, and M. Thullner. Anthropogenic perturbation of the carbon fluxes from land to ocean. Nature Geoscience **6:** 597-607. 2013.

Reuer, M. K., B. A. Barnett, M. L. Bender, P. G. Falkowski, and M. B. Hendricks. New estimates of Southern Ocean biological production rates from O_2/Ar ratios and the triple isotope composition of O_2. Deep-Sea Research Part I-Oceanographic Research Papers **54:** 951-974. 2007.

Roberts, B. J., and S. M. Doty. Spatial and temporal patterns of benthic respiration and net nutrient fluxes in the Atchafalaya River Delta Estuary. Estuaries and Coasts **38:** 1918-1936. 2015.

Sambrotto, R. N., G. Savidge, C. Robinson, P. Boyd, T. Takahashi, D. M. Karl, C. Langdon, D. Chipman, J. Marra, and L. Codispoti. Elevated consumption of carbon relative to nitrogen in the surface ocean. Nature **363:** 248-250. 1993.

Sarmiento, J. L., and N. Gruber. Ocean Biogeochemical Dynamics. Princeton University Press. 2006.

Seguro, I., García, C. M., Papaspyrou, S., Gálvez, J. A., García-Robledo, E., Navarro, G., Soria-Píriz, S., Aguilar, V., Lizano, O. G., Morales-Ramírez, A., and Corzo, A.: Seasonal changes of the microplankton community along a tropical estuary, Regional Studies in Marine Science, **2**, 189-202, 2015.

Shadwick, E. H., B. Tilbrook, N. Cassar, T. W. Trull, and S. R. Rintoul. Summertime physical and biological controls on O_2 and CO_2 in the Australian Sector of the Southern Ocean. Journal of Marine Systems **147:** 21-28. 2015.

Sweeney, C., E. Gloor, A. R. Jacobson, R. M. Key, G. Mckinley, J. L. Sarmiento, and R. Wanninkhof. Constraining global air-sea gas exchange for CO_2 with recent bomb ^{14}C measurements. Global Biogeochemical Cycles **21**(2): GB2015. 2007.

Teeter, L., Hamme, R. C., Ianson, D., and Bianucci, L. Accurate estimation of net community production from O_2/Ar measurements. Global Biogeochemical Cycles, 32, 1163–1181. https://doi.org/10.1029/2017GB005874. 2018.

Ternon, J. F., C. Oudot, A. Dessier, and D. Diverres. A seasonal tropical sink for atmospheric CO_2 in the Atlantic ocean: the role of the Amazon River discharge. Marine Chemistry **68:** 183-201. 2000.

Turner, R. E., and N. N. Rabalais. Nitrogen and phosphorus phytoplankton growth limitation in the northern Gulf of Mexico. Aquatic Microbial Ecology **68:** 159-169. 2013.

Turner, R. E., N. N. Rabalais, and D. Justic. Predicting summer hypoxia in the northern Gulf of Mexico: Redux. Marine Pollution Bulletin **64:** 319-324. 2012.

Ulfsbo, A., N. Cassar, M. Korhonen, S. Van Heuven, M. Hoppema, G. Kattner, and L. G. Anderson. Late summer net community production in the central Arctic Ocean using multiple approaches. Global Biogeochemical Cycles **28:** 1129-1148. 2014.

Wallace, R. B., H. Baumann, J. S. Grear, R. C. Aller, and C. J. Gobler. Coastal ocean acidification: The other eutrophication problem. Estuarine Coastal and Shelf Science **148:** 1-13. 2014.

Weiss, R. F. Carbon dioxide in water and seawater: the solubility of a non-ideal gas, p. 203-215. Marine Chemistry. 1974.

Wolf-Gladrow, D. A., R. E. Zeebe, C. Klaas, A. Kortzinger, and A. G. Dickson. Total alkalinity: The explicit conservative expression and its application to biogeochemical processes. Marine Chemistry **106**(1-2): 287-300. 2007.

Xue, J. H., W. J. Cai, X. P. Hu, W. J. Huang, S. E. Lohrenz, and K. Gundersen. Temporal variation and stoichiometric ratios of

organic matter remineralization in bottom waters of the northern Gulf of Mexico during late spring and summer. Journal of Geophysical Research-Oceans **120:** 8304-8326. 2015.

Xue, Z., R. He, K. Fennel, W. J. Cai, S. Lohrenz, and C. Hopkinson. Modeling ocean circulation and biogeochemical variability in the Gulf of Mexico. Biogeosciences **10:** 7219-7234. 2013.

5   Xue, Z., R. Y. He, K. Fennel, W. J. Cai, S. Lohrenz, W. J. Huang, H. Q. Tian, W. Ren, and Z. C. Zang. Modeling pCO$_2$ variability in the Gulf of Mexico. Biogeosciences **13:** 4359-4377. 2016.

Yang, X. F., L. Xue, Y. X. Li, P. Han, X. Y. Liu, L. J. Zhang, and W. J. Cai. Treated wastewater changes the export of dissolved inorganic carbon and its isotopic composition and leads to acidification in coastal oceans. Environmental Science & Technology **52:** 5590-5599. 2018.

10   Zeebe, R. E., and D. Wolf-Gladrow. CO$_2$ in seawater: Equilibrium, kinetics, isotopes., Elsevier, Amsterdam. 2001.

Zhang, X. Q., R. D. Hetland, M. Marta-Almeida, and S. F. Dimarco. A numerical investigation of the Mississippi and Atchafalaya freshwater transport, filling and flushing times on the Texas-Louisiana Shelf. Journal of Geophysical Research-Oceans **117**(C11). 2012.

Table

Table 1 The end-member properties used in the three end-member mixing model.

End-member	Salinity	TA (μmol kg^{-1})	DIC (μmol kg^{-1})	NO$_x$ (μmol kg^{-1})
Atchafalaya River	0	2091	2128	113.14
Mississippi River	0	2314	2312	123.27
Gulf surface seawater	36.15	2407	2076	0.44

Figure
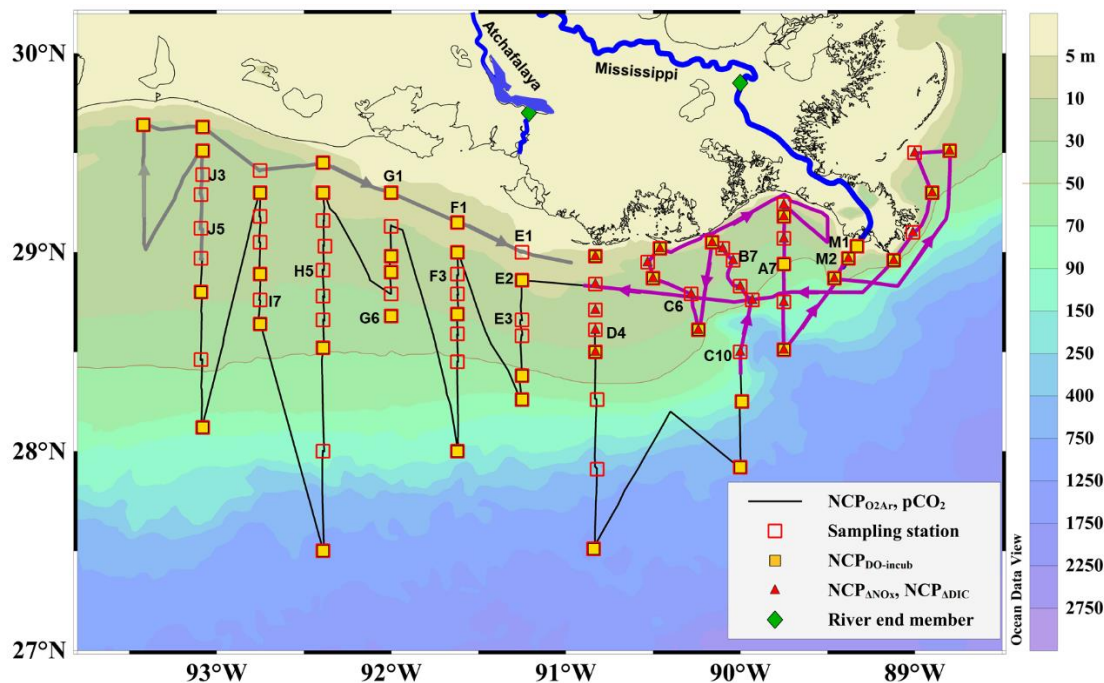
Fig. 1. Map and sampling sites in the northern Gulf of Mexico during the April 2017 cruise. The black dotted line is the cruise track along which the high-resolution underway measurements were made. The track in the Mississippi plume (purple line, 8-11 April) and in the Atchafalaya coastal regions (grey line, 15-17 April) are highlighted. Also shown are the 83 CTD sampling stations (hollow red squares), the 43 stations where light/dark bottle DO incubations were conducted (solid yellow squares), the 30 stations where non-conservative changes in DIC and NO$_x$ were used to estimate NCP rates (solid red triangles), and the 2 stations where the properties of river end-members were measured (solid green diamonds). The vertical CTD profiles of the labelled stations were shown in the supplement.
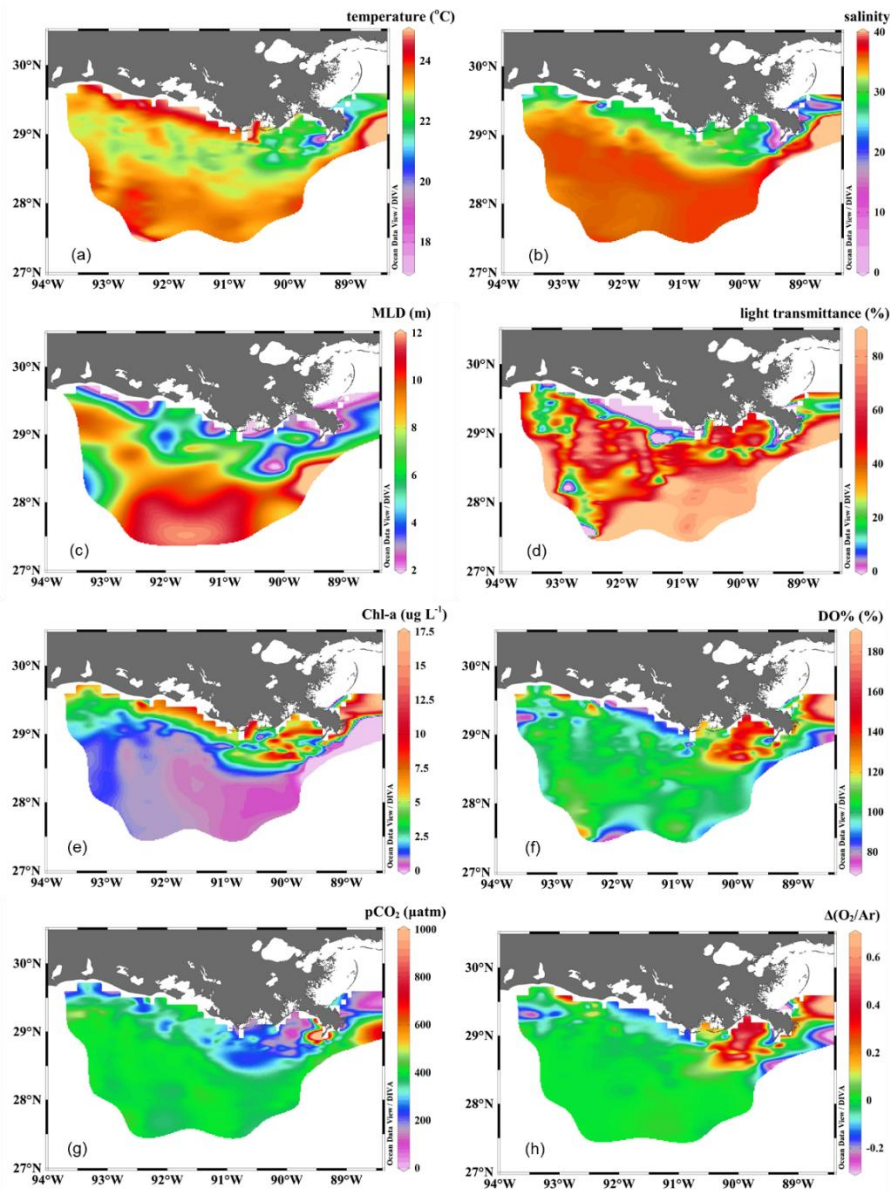
Fig. 2. The distribution of (a) temperature, (b) salinity, (c) mixed layer depth (MLD), (d) light transmittance, (e) chlorophyll-a concentration (Chl-a), (f) oxygen saturation percentage (DO%), (g) partial pressure of CO_2 (pCO_2), and (h) biologically induced oxygen supersaturation ($\Delta O_2/Ar$) in the surface water of the nGOM.
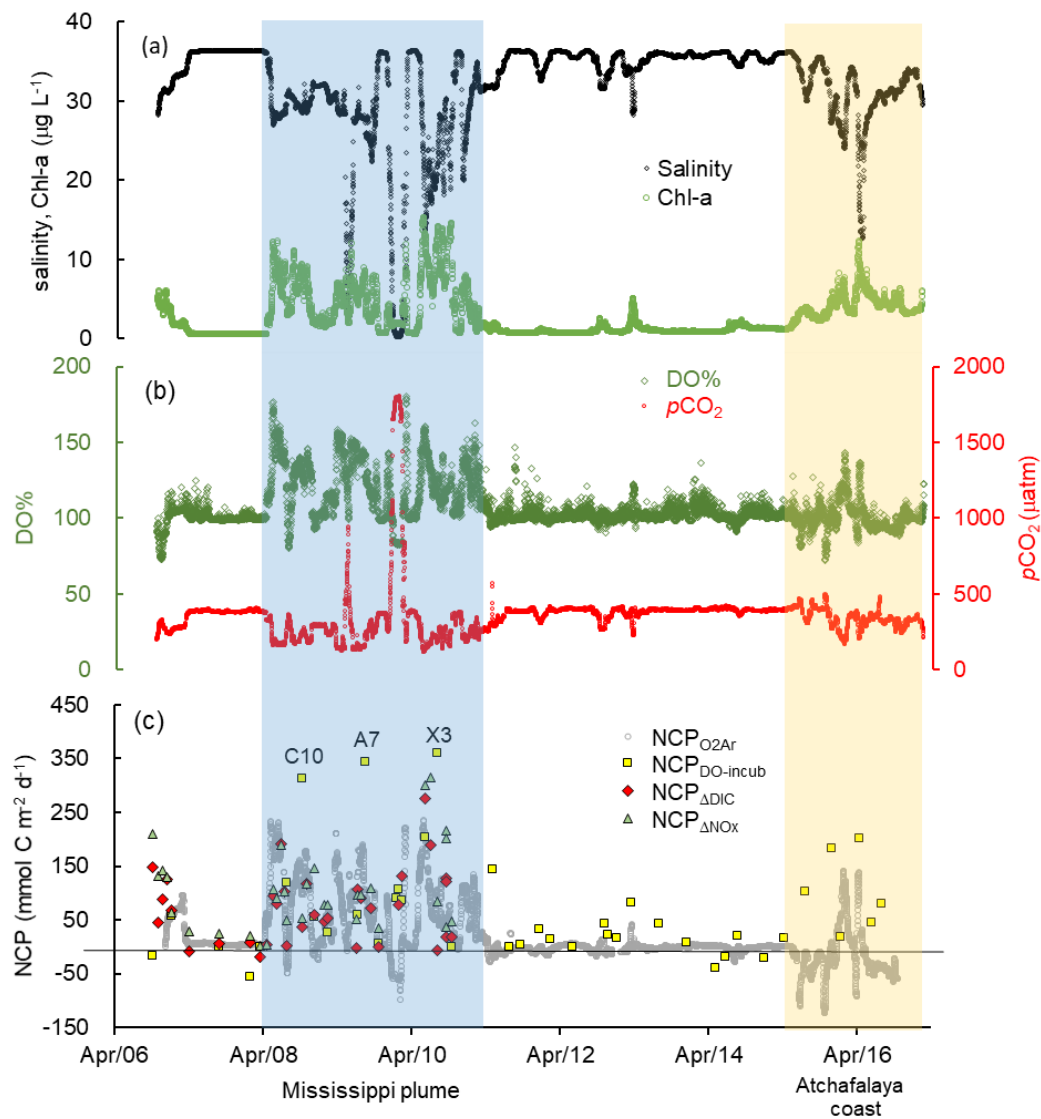
Fig. 3. The underway measurements of (a) salinity and Chl-a, (b) DO% and pCO_2, and (c) NCP rates estimated from the O$_2$/Ar measurement (NCP$_{O2Ar}$, grey circles). Also shown in panel c are the NCP rates estimated from the light/dark DO incubation (NCP$_{DO-incub}$, yellow squares), non-conservative changes in DIC (NCP$_{\Delta DIC}$, red diamonds) or NO$_x$ (NCP$_{\Delta NOx}$, green triangles). See Figure 1 for the cruise track in the Mississippi plume (8-11 April) and Atchafalaya coast (15-17 April). See Figure 5 for the positions of stations C10, A7, and X3 in the Mississippi plume.
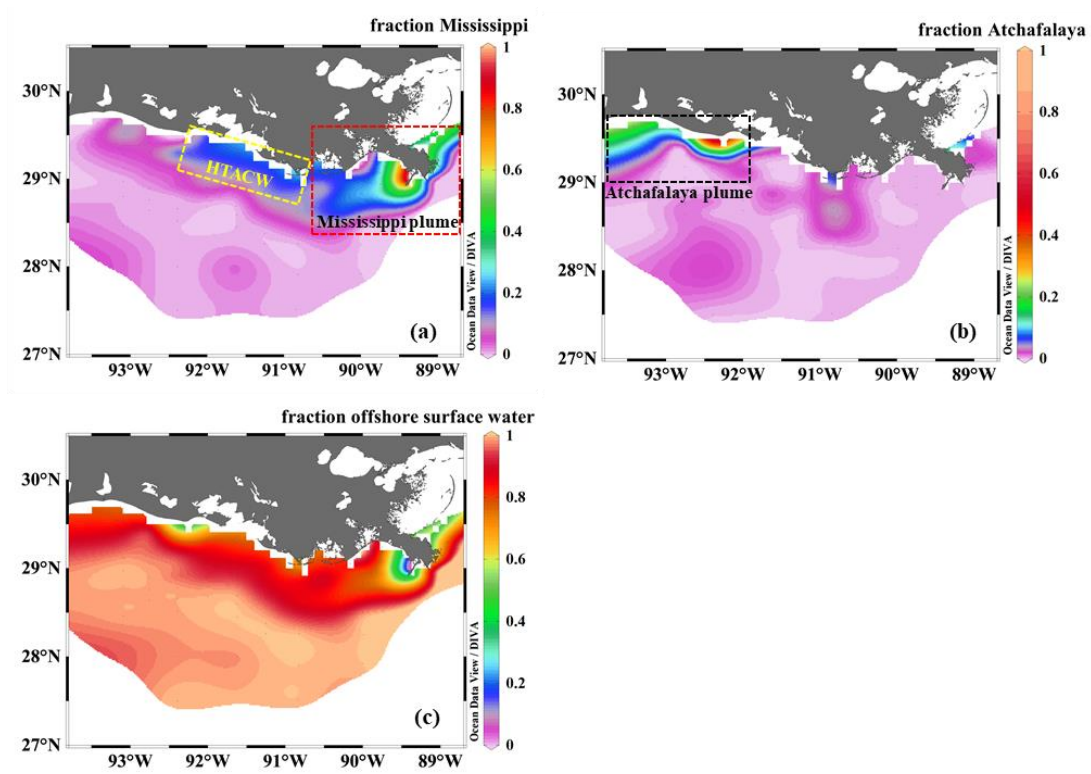
Fig. 4. The fractional contribution of (a) the Mississippi River, (b) the Atchafalaya River, and (c) offshore surface water to the surface water of the nGOM estimated from the three end-member mixing model. The sub-regions shown in panels (a) and (b) are the Mississippi plume, the high-turbidity Atchafalaya coastal water (HTACW), and the Atchafalaya plume.

5
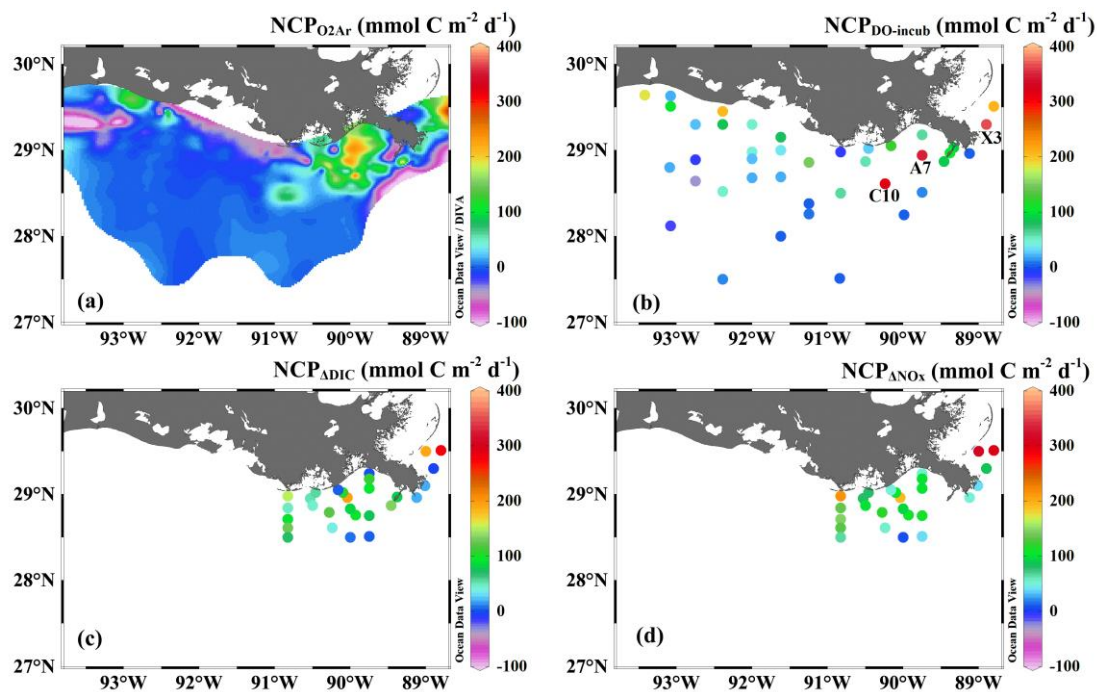
Fig. 5. The spatial variability of (a) NCP_{O2Ar}, (b) $NCP_{DO\text{-}incub}$, (c) $NCP_{\Delta DIC}$, and (d) $NCP_{\Delta NOx}$. Noted that $NCP_{\Delta DIC}$ and $NCP_{\Delta NOx}$ were only estimated in the Mississippi plume (panels c, d).
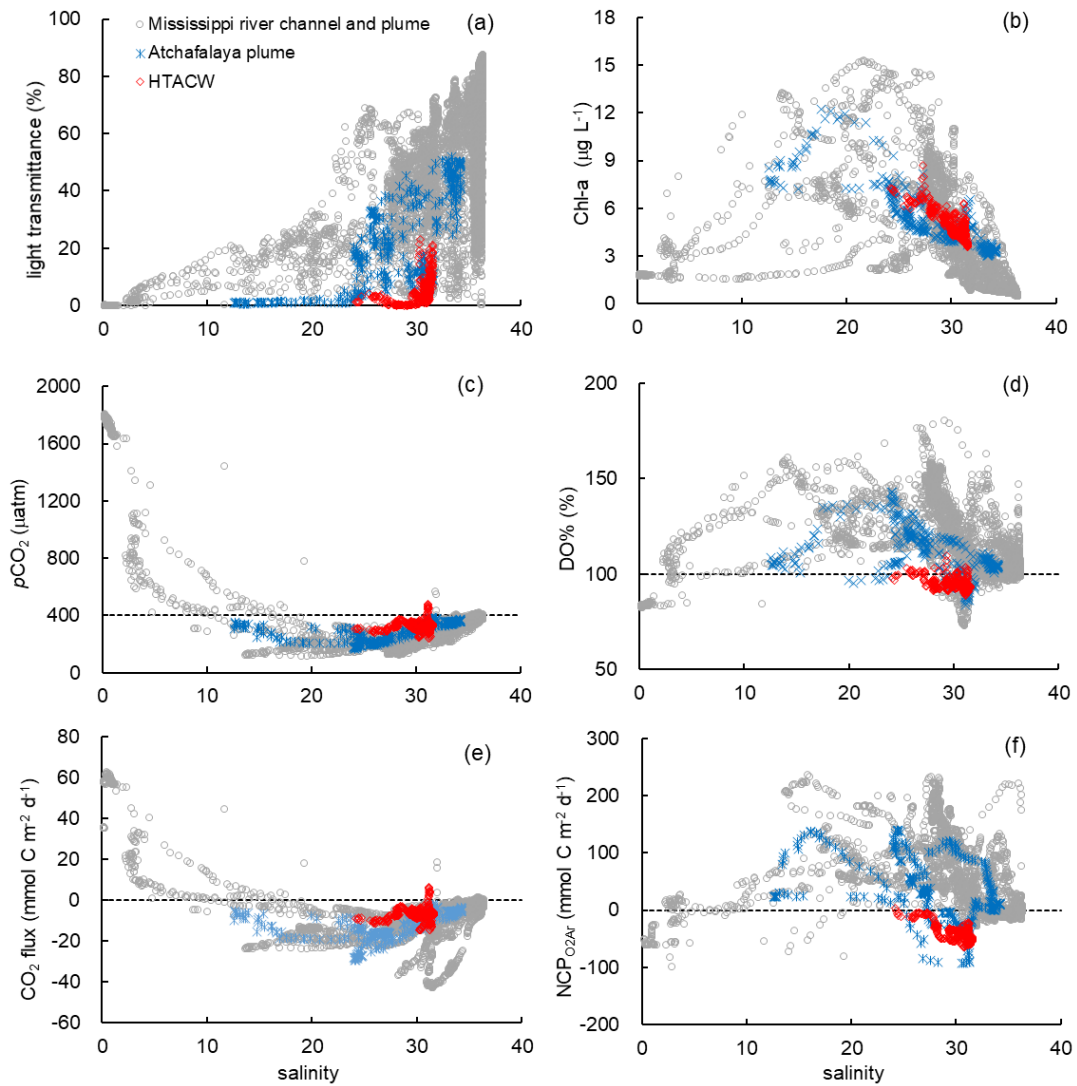
Fig. 6. The distribution of (a) light transmittance, (b) Chl-a, (c) pCO_2, (d) DO%, (e) CO_2 flux, and (f) NCP_{O2Ar} along the salinity gradient in different sub-regions. The dash lines in panels c to f are the atmospheric pCO_2 (405 µatm), DO% of 100 %, zero CO_2 flux, and zero NCP_{O2Ar} respectively.
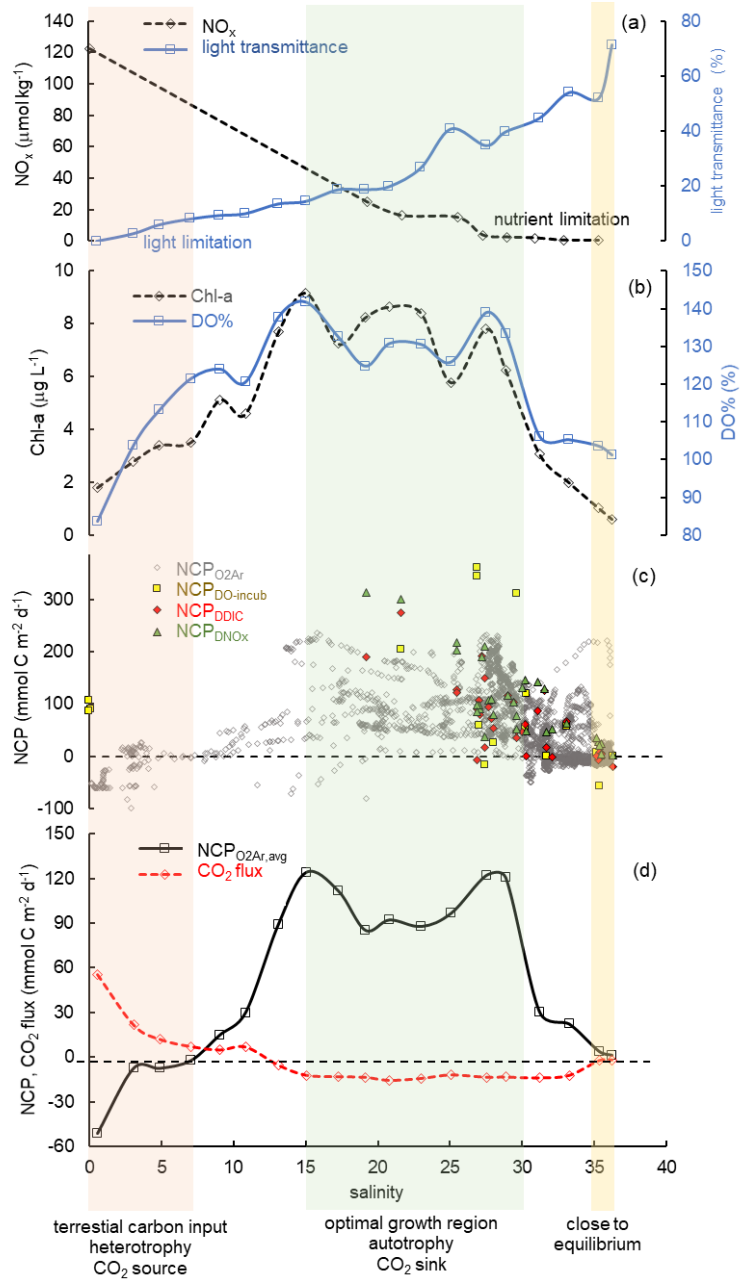
Fig. 7. The distribution of (a) NO_x and light transmittance, (b) Chl-a and DO%, (c) NCP estimated from various methods, and (d) NCP_{O2Ar} and CO_2 flux along the salinity gradient in the Mississippi plume. Data in panels (a), (b), and (d) were averaged over increments of two salinity units.
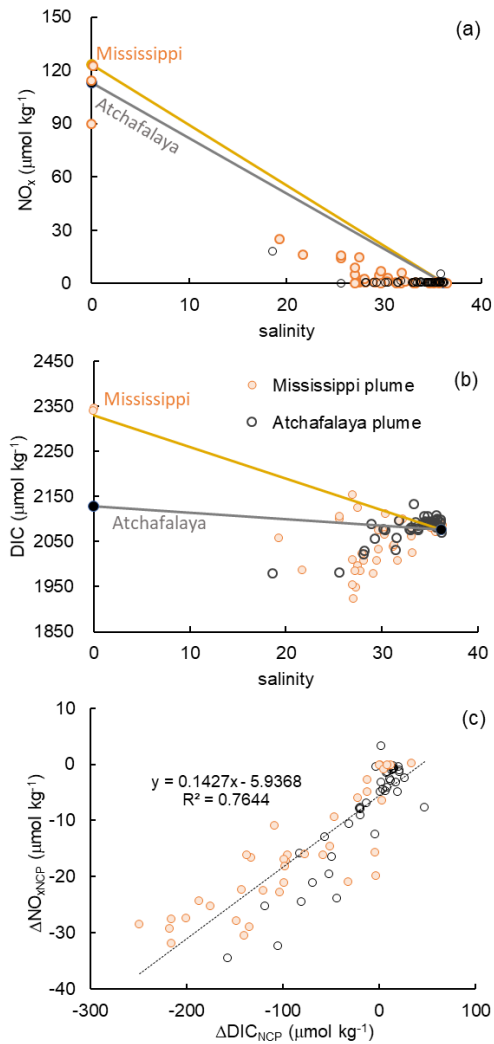
5

Fig. 8. Scatter plots of (a) DIC and salinity, (b) NO_x and salinity, and (c) the non-conservative changes in DIC (ΔDIC_{NCP}) and NO_x (ΔNO_{xNCP}) in the Mississippi and Atchafalaya plumes. The end-member concentrations of the Mississippi river, the Atchafalaya River, and offshore gulf surface water are shown in panels (a) and (b) together with the conservative mixing lines.
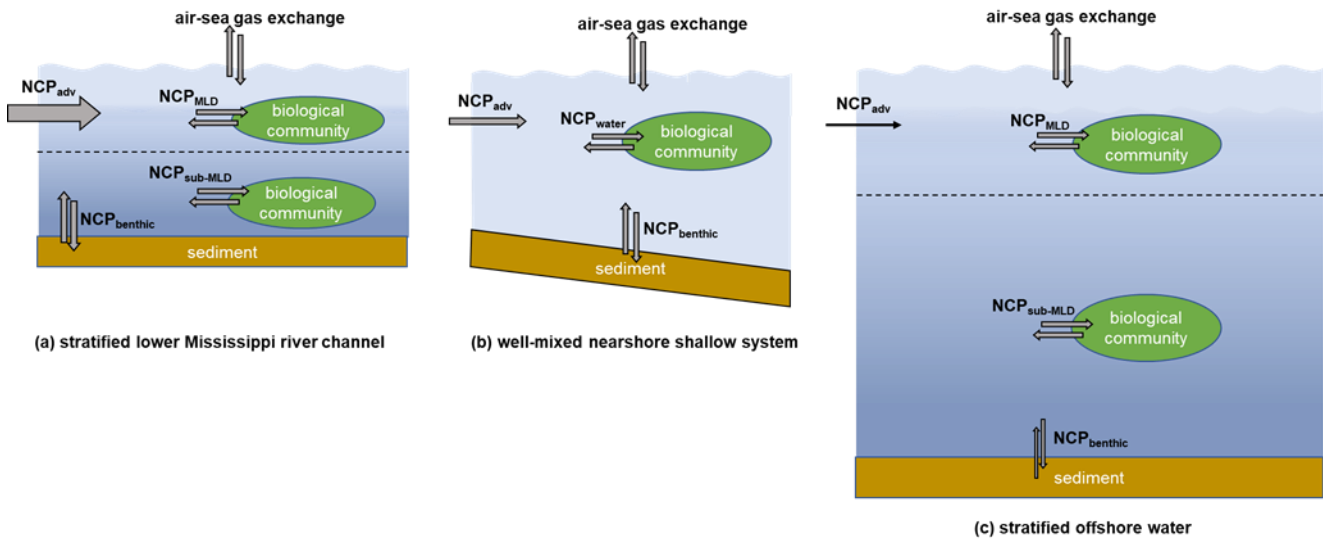
5

Fig. 9. The differences in water column mixing conditions in the nGOM and their influences on NCP estimation. The dotted lines in panels (a) and (c) indicate the mixed layer depth. In the stratified lower Mississippi River channel (a) and the offshore stratified system (c), $NCP_{DO-incub}$ equals the *in situ* community production in the mixed layer (NCP_{MLD}), while NCP_{O2Ar} reflects the combined result of the NCP_{MLD} and the influence of lateral advection of the river water (NCP_{adv}). In the nearshore well-mixed shallow system (b), $NCP_{DO-incub}$ equals the water column community production (NCP_{water}), while NCP_{O2Ar} reflects the combined result of NCP_{water}, $NCP_{benthic}$, and NCP_{adv}. Note that the influence of NCP_{adv} decreases offshore with the increasing water residence time.
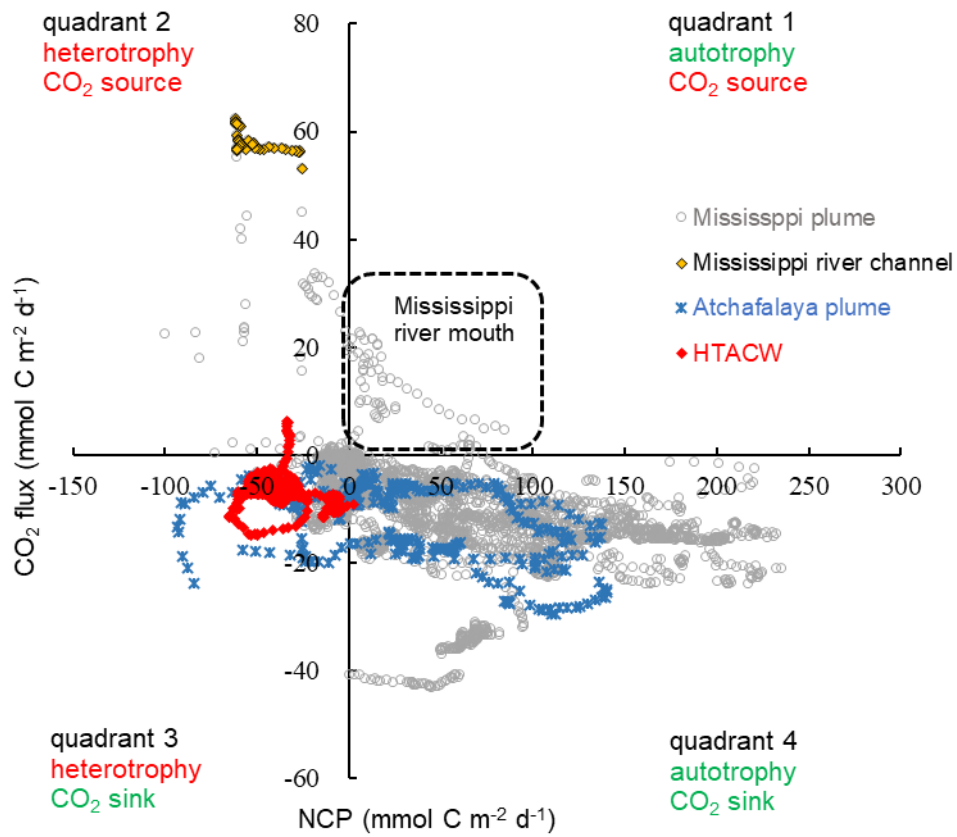
Fig. 10. Scatter plot of NCP$_{O2Ar}$ and CO_2 flux observed in the surface water of the nGOM. Positive NCP implies net autotrophy and negative CO_2 flux implies net oceanic CO_2 uptake from the atmosphere.
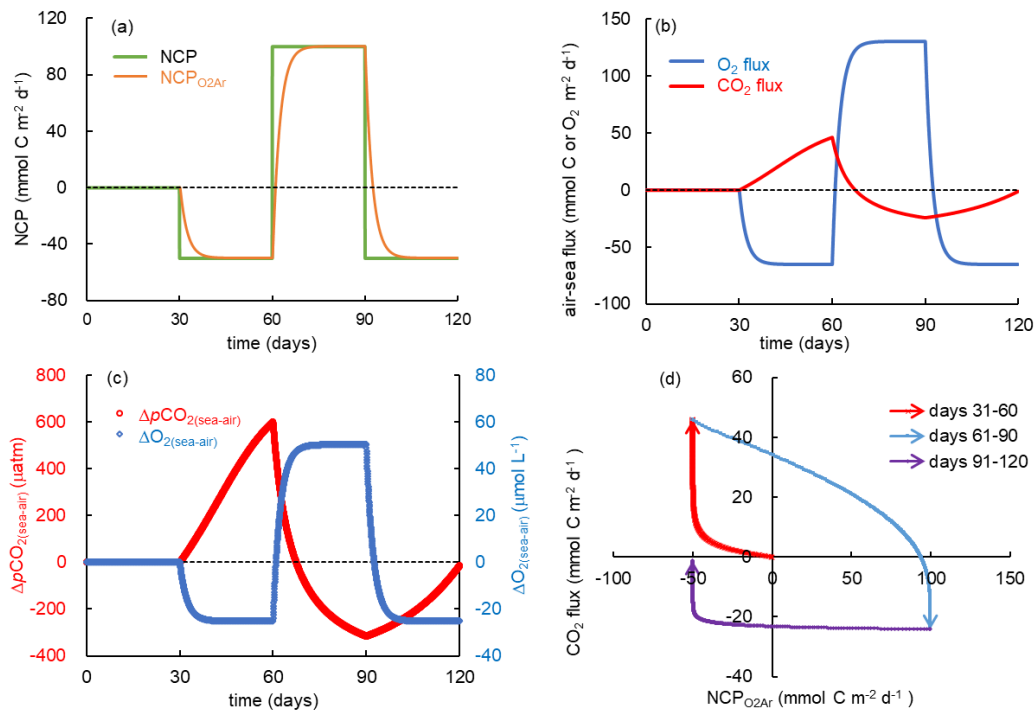
Fig. 11. Simulation of carbon and oxygen dynamics responding to time-dependent varying NCP rates and gas exchange using a box model. The variations of (a) NCP and exponentially weighted NCP (NCP_{O2Ar}), (b) air-sea CO_2 flux and O_2 flux, and (c) air-sea pCO_2 difference ($\Delta pCO_{2(sea-air)}$) and O_2 difference ($\Delta O_{2(sea-air)}$). (d) Scatter plot of CO_2 flux and NCP_{O2Ar}. Positive NCP implies net autotrophy and negative O_2 and CO_2 fluxes implies gas influxes into the water. See the text for details.